

# Benzene in a high-intensity high-frequency circularly polarized laser

R.Mythreyi

*A dissertation submitted for the partial fulfillment of  
BS-MS dual degree in Science*



INDIAN INSTITUTE OF SCIENCE EDUCATION AND  
RESEARCH, MOHALI

April 2019

## Certificate of Examination

This is to certify that the dissertation titled “**Benzene in a high-intensity high-frequency circularly polarized laser**” submitted by **Ms. R. Mythreyi (Reg. No. MS14102)** for the partial fulfillment of BS-MS dual degree program of the Institute, has been examined by the thesis committee duly appointed by the Institute. The committee finds the work done by the candidate satisfactory and recommends that the report be accepted.

Professor K. S. Viswanathan

Dr. Kamal P. Singh

Dr. P. Balanarayan  
(Supervisor)

## Declaration

The work presented in this dissertation has been carried out by me with Dr. P. Balanarayan at the Indian Institute of Science Education and Research, Mohali. This work has not been submitted in part or in full for a degree, a diploma, or a fellowship to any other university or institute. Whenever contributions of others are involved, every effort is made to indicate this clearly, with due acknowledgement of collaborative research and discussions. This thesis is a bonafide record of original work done by me and all sources listed within have been detailed in the bibliography.

R.Mythreyi

(MS14102)

Dated: 26/04/2019

In my capacity as the supervisor of the candidates project work, I certify that the above statements by the candidate are true to the best of my knowledge.

Dr. P. Balanarayan

(Supervisor)

# Acknowledgements

I would like to express my gratitude to my advisor, Dr. P. Balanarayan, for his support and guidance throughout my project. I would also like to thank my project committee members, Professor K. S. Viswanathan and Dr. Kamal P. Singh for reading drafts of this dissertation and providing many valuable comments that improved the contents of this dissertation. I am thankful to Prashant, Nitin, Mishu, Naveen, Prateek, Alkit, Taseng, Vishal, Rishabh, Shivam, Sandeep for their inputs, discussions and cheerful company through the period of this project. I am especially thankful to Prashant, for helping me throughout this work with the codes and computations and Mishu, for correcting the thesis. I am grateful to my family for having always been loving, supportive and encouraging. I thank my friends Shantanu, Mrudula, Geeta and Deepali for their constant company and support through these five years.

*“The very powerful and the very stupid have one thing in common. They don’t alter their views to fit the facts. They alter the facts to fit their views.”*

The 4th Doctor,  
*Doctor Who*

*Dedicated to my family, friends and teachers*

# Contents

<b>Acknowledgements</b>	<b>iii</b>
<b>List of Figures</b>	<b>viii</b>
<b>Abbreviations</b>	<b>xi</b>
<b>Physical Constants</b>	<b>xii</b>
<b>1 Introduction</b>	<b>1</b>
1.1 Light-matter interaction and the Time-Dependent Schrödinger equation . . . . .	2
1.1.1 Gauge invariance . . . . .	2
1.1.2 Dipole approximation . . . . .	4
1.2 Ionization processes in intense fields . . . . .	5
1.3 The Kramers-Henneberger atom . . . . .	6
1.3.1 Polarization . . . . .	7
1.4 Electronic structure of benzene . . . . .	9
1.4.1 Benzene and graphene . . . . .	11
1.5 Thesis outline . . . . .	13
<b>2 Kramers-Henneberger potentials, states of model and atomic systems in a circularly polarized pulse</b>	<b>16</b>
2.1 Kramers-Henneberger transformation . . . . .	16
2.1.1 Kramers-Henneberger potential . . . . .	18
2.2 Model potential and hydrogen atom . . . . .	19
2.3 Methodology . . . . .	21
2.4 Even-tempered Gaussian basis set . . . . .	21
2.5 KH states of helium . . . . .	23
2.6 KH states of carbon . . . . .	24
<b>3 Benzene in a circularly polarized pulse</b>	<b>27</b>
3.1 Kramers-Henneberger potential of benzene . . . . .	27
3.1.1 Kramers-Henneberger states of benzene . . . . .	30
3.2 Conclusion . . . . .	34

---

<b>A Atomic units</b>	<b>35</b>
A.1 Energy conversion . . . . .	35
<b>B SPD-type basis set</b>	<b>36</b>
B.1 Helium . . . . .	36

# List of Figures

1.1	a) Linearly polarized field $E_0 \cos(\omega t)\hat{x}$ b) Circularly polarized field along x-y axes $E_0(\cos \omega t\hat{x} + \sin \omega t\hat{y})$ c) Elliptically polarized field along x-y axes $E_{0_1} \cos \omega t\hat{x} + E_{0_2} \sin \omega t\hat{y}$ ; $E_0$ is the amplitude of the field and $\omega$ is its frequency. The linearly polarized field is seen to oscillate only along the $x$ axis while the circularly and elliptically polarized fields oscillate along the $x$ and $y$ axes with equal amplitudes and unequal amplitudes respectively along both the directions. . . . .	8
1.2	Hartree-Fock $\pi$ MOs of benzene calculated using 6-311++g** basis set arranged in an ascending order of energy. The occupancy of these orbitals is depicted schematically using arrows (each arrow represents an electron). The lowest three orbitals are the bonding $\pi$ orbitals which hold a total of six $\pi$ electrons. The higher three orbitals are the anti-bonding $\pi$ orbitals. The energy of the orbitals is seen to increase as the number of nodal planes increase as 1,2,3 and 4. MOs having the same number of nodal planes are degenerate. . . . .	10
1.3	A graphical representation of the energy levels of benzene using the <i>polygon method</i> ; $\alpha$ is the energy of an electron in the $2p$ orbital and $\beta$ is the interaction energy between two electrons in two $2p$ orbitals. (both are conventionally negative). This method easily helps to find out the number of bonding and anti-bonding $\pi$ orbitals, the energy levels of these orbitals and the number of degenerate orbitals. . . . .	11
1.4	Energy curve for proton transfer through benzene using the 6-311++g** basis set and MP2 level of theory. This curve was obtained by using Gaussian09 for 401 points. A barrier is seen when the proton sits right at the center of benzene and a minimum is obtained when the proton is exactly above and below benzene respectively. . . . .	12
2.1	Contours of $V_n^{KH}(\vec{r})$ for the model potential $n=0-5$ calculated according to Eq. [2.18]. $V_0^{KH}$ contour is a circle with zero nodes. As $n$ increases, the number of nodal planes increase as $n-1$ . Red and blue stand for positive and negative potential values respectively. . . . .	20
2.2	The isosurface of $V_0^{KH}$ for hydrogen at an isovalue = -3.7207 a.u. visualized using VMD. [3] The potential oscillates in a circular motion to give a ring shaped time-averaged potential. The ring like structure implies there is no potential at the center for this isovalue. . . . .	21
2.3	A flow chart explaining the steps to calculate the KH potentials and energies. 22	

2.4	Helium 1s Hartree-Fock orbital at $\alpha_0 = 0.0$ a.u. and the ring shaped KH orbital at $\alpha_0 = 2.94$ a.u. at isovalues (i) 0.008782, (ii) 0.022298, (iii) 0.029056 and (iv) 0.030454 calculated using the SPD-type basis set. From the lowest isovalue itself, we see a dip in the center of the orbital. The second isovalue shows an elongation of the orbital. For the third isovalue, we can see the ring begins to show and the ring is clearly seen for the maximum isovalue. . . . .	23
2.5	The Hartree-Fock KH energies ( $E^{KH}$ ) (a.u.) of the KH states of helium with varying $\alpha_0$ . The basis set used was the SPD-type basis set given in Appendix A. The ground state energy at $\alpha_0 = 0$ is -2.90212 a.u. The rise in energy is sharp for $\alpha_0 > 1$ . At 1, there is a discontinuity in the plot which could have occurred due to the basis. Beyond 1, the rise in energy is comparatively slow. . . . .	24
2.6	Occupied orbitals of the carbon atom at a) $\alpha_0 = 0.0$ a.u. and b) $\alpha_0 = 3.0$ a.u. calculated using the SPD-type basis set at the Hartree-Fock level of theory. As $\alpha_0$ increases, the core 1s orbital goes from a sphere to a “doughnut” shape and the 2s and 2p orbitals no longer exist; we instead get <i>d</i> type degenerate orbitals with two nodal planes each. . . . .	25
2.7	Hartree-Fock KH energies calculated for 10 $\alpha_0$ values for the carbon atom. The ground state energy at $\alpha_0$ is -37.422 a.u. Similar to helium, the energy initially shows a sharp increase in energy for $\alpha_0$ up to 1 a.u. and then gradually increases. . . . .	25
3.1	A schematic diagram showing varying radii of the six circles (potentials) for varying $\alpha_0$ . $\alpha_0 = \text{Radius of the circle}$ . The radius of each circle increases on increasing the $\alpha_0$ value. In the last diagram, we see that the radius of the circle equals the side of the hexagon; this gives an intersection of all the six circles in the center which would give a deep minimum. This means that most of the electrons will be held here. . . . .	28
3.2	Isosurfaces of the higher order harmonics of benzene $V_n^{KH}(\vec{r})$ for $n = 1-5$ calculated according to the Eq.[3.1]. These potentials were visualized at an isovalue of $ \pm 1 $ . . . . .	28
3.3	a) Isosurfaces calculated at isovalues 1a) 19.6 a.u., 2a) -19.8801 a.u. and 3a) 18.4462 a.u. and b) 2D plots of $V_0^{KH}$ for $\alpha_0 = (1) 2.3$ a.u. (2) 2.7 a.u. (3) 3.0 a.u. Visualization of the isosurfaces was done with the help of VMD. The isosurface is maximum at the center at $\alpha_0 = 2.7$ a.u. (in the red box) close to the C-C bond distance value of 2.67 a.u. As we increase and decrease the $\alpha_0$ values, the maximum shifts away from the center. The plot of the potential shows the same idea graphically. The local minima in each graph arise due to the intersection of two carbon atoms (can be seen from the schematic diagram). . . . .	29
3.4	a) Isosurfaces of molecular orbitals and b) Electronic density of benzene (visualized using VMD) with increasing $\alpha_0$ . The first and the last three occupied molecular orbitals (in order of increasing energy) are shown on the left side along with the total electronic density for each $\alpha_0$ on the right side. The electronic density increases towards the center with increasing $\alpha_0$ and is maximum at the center for $\alpha_0 = 2.7$ a.u.(the red box). This is the same value for which we saw a deep minimum in the KH potential in the previous section. The core molecular orbital follows the exact same trend as the electronic density. . . . .	31

- 
- 3.5 Hartree-Fock energies of benzene vs  $\alpha_0$  calculated using the SPD-type basis set mentioned in the previous chapter. For  $\alpha_0$  below 0.5 a.u., the energy increases rapidly as compared to the rate of increase for values greater than 0.5 a.u. As  $\alpha_0$  goes to 3.5 a.u., energy tends to 0. . . . . 32
- 3.6 Orbital energies vs  $\alpha_0$  The increase in energy in the core orbitals follows the same trend as HF energies. Relatively, the remaining occupied orbitals show a much smaller change in energy. This implies that changes in the core orbitals significantly affect the total energy of the molecule. . . . . 32
- 3.7 CIS energies as a function of  $\alpha_0$  for the first 20 singly excited states of benzene at each  $\alpha_0$ . This plot looks exactly similar to the plot of Hartree-Fock energies and does not show the excited state energies clearly. This is because the relative difference of the excited state energies is very small (of the order of magnitude -1 to -2 a.u.) compared to the magnitude of the ground state energies at each  $\alpha_0$ . Hence, it makes sense to look at the excited state energies relative to the ground state in order to understand the plot. . . . . 33
- 3.8 CIS calculations for benzene done using GAMESS and the SPD-type basis set. Number of valence orbitals were taken to be 100 and the the number of CSFs were 2101. The energies plotted here are obtained after taking a difference of the excited states with respect to the ground state. This had to be done since the range of the energies was very large compared to the increase in energies of the excited states. . . . . 33

# Abbreviations

<b>a.u.</b>	atomic <b>u</b> its
<b>CW</b>	Continuous <b>W</b> ave
<b>MPI</b>	Multi <b>P</b> hoton Ionization
<b>VMD</b>	Visual <b>M</b> olecular <b>D</b> ynamics
<b>CIS</b>	Configuration Interaction <b>S</b> ingles
<b>TISE</b>	Time Independent <b>S</b> chrödinger <b>E</b> quation
<b>TDSE</b>	Time <b>D</b> ependent <b>S</b> chrödinger <b>E</b> quation

# Physical Constants

Speed of Light	$c$	$=$	$2.997\,924\,58 \times 10^8 \text{ ms}^{-1}$	(exact)
Electron rest mass	$m_e$	$=$	$9.10938291 \times 10^{-31} \text{ kg}$	
Electron charge	$e$	$=$	$1.60217657 \times 10^{-19} \text{ C}$	
Planck's constant	$h$	$=$	$6.62607004 \times 10^{-34} \text{ m}^2 \text{ kgs}$	
Vacuum permittivity	$\epsilon_0$	$=$	$8.854187.. \times 10^{-12} \text{ Fm}^{-1}$	(approximate)

## Abstract

Atomic and molecular stabilization in extremely intense laser fields has been studied extensively over the past few years in the field of laser-atom physics. Though this might sound counter-intuitive to the process of ionization, there have been a number of theoretical studies to prove this idea and a few recent experiments which give direct evidence of this concept. Here, we examine this phenomenon of stabilization in the high-intensity regime for benzene using a circularly polarized pulse. Atoms have been studied previously in a circularly polarized pulse and their behavior suggests an interesting outcome for benzene. One of the applications of this outcome could be to gain a temporal control over proton migration through the center of benzene provided we use the right set of laser parameters. This is a fascinating phenomenon to think of when we remember that there is a  $\pi$  electron cloud above and below the ring due to which the field free benzene molecule will not hold the proton at the center.

# Chapter 1

## Introduction

The wave-particle duality of light and matter has been studied extensively since its discovery in the 20th century. Although the electromagnetic theory of light, proposed by Faraday and studied by Maxwell in the 19th century, gave rise to many new inventions like the radio, television and wireless communications, it was not sufficient to describe other visual effects of light such as spectral lines. The development of quantum theory of light by Max Planck in the 20th century was necessary to describe the interactions of light with matter at an atomic and molecular scale. Later, experiments such as two-slit interference and diffraction of electrons showed that even electrons could be both particles and waves giving rise to the branch of quantum mechanics. Quantum mechanics looks at the wave nature of particles like electrons. The equation of motion for the electron is given by the Time-Dependent Schrödinger equation,

$$i\hbar\frac{\partial\Psi}{\partial t} = \hat{H}\Psi \quad (1.1)$$

where  $i$  is the imaginary unit,  $\hbar = h/2\pi$  and  $h$  is Planck's constant,  $\hat{H}$  is the Hamiltonian operator for the observable, energy, and  $\Psi$  is the wavefunction of the electron which contains all the information about the electron. The forthcoming section describes the nature of a Hamiltonian when electrons interact with light.

## 1.1 Light-matter interaction and the Time-Dependent Schrödinger equation

There are three different approaches to explain the phenomena arising due to light-matter interaction - classical, semi-classical and quantum mechanical descriptions. In the semi-classical theory, light is treated as an electromagnetic wave and the atoms are quantum mechanical objects. In the quantum approach, light and atoms are quantized using field theory. Semi-classical methods are widely used to understand absorption and scattering while the quantum methods have more recently been developed to understand processes such as spontaneous emission and Lamb shift. [1] In this thesis, a semi-classical approach is followed which is sufficient to understand the behavior of atoms and molecules in the presence of time varying strong fields.

In order to understand the effect of intense electromagnetic fields on particles, the form of the Hamiltonian defines the system under study.

### 1.1.1 Gauge invariance

The Time-Dependent Schrödinger equation (TDSE) for an electron in an atom in an oscillating electric field is:

$$i\hbar \frac{\partial \Psi}{\partial t} = \hat{H} \Psi \quad (1.2)$$

$$\hat{H} = \frac{1}{2m_e} \left[ \vec{p} - \frac{e}{c} \vec{A}(\vec{r}, t) \right]^2 + e\phi + V(\vec{r}) \quad (1.3)$$

where  $m_e$  is the mass of the electron,  $\vec{p}$  is the electron momentum operator,  $e$  is the charge of the electron,  $V(\vec{r})$  is the binding potential of the atom and  $\vec{A}$  and  $\phi$  are known as vector and scalar potentials respectively.

Scalar potential is the term given to any scalar function which is the gradient of a curl-less field and vector potential is the term given to any vector function which is the curl of a divergence-less field. [2] The vector and scalar potentials  $\vec{A}$  and  $\phi$  are gauge dependent quantities. They change across different gauge transformations to keep the total system invariant under these transformations. From Maxwell's equations, we know that

$$\vec{\nabla} \cdot \vec{B} = 0 \quad (1.4)$$

$$\vec{\nabla} \times \vec{E} + \partial \vec{B} / \partial t = 0 \quad (1.5)$$

Differential calculus tells us that the divergence of a curl and that the curl of a gradient are always zero. Hence, we can write  $\vec{B} = \vec{\nabla} \times \vec{A}$ . Substituting this in the second Maxwell's equation above, we get  $\vec{E} = -\vec{\nabla}\phi - \frac{1}{c}\frac{\partial\vec{A}}{\partial t}$ .  $\vec{A}$  and  $\phi$  do not uniquely specify  $\vec{E}$  and  $\vec{B}$ . They can be written as

$$\vec{A}' = \vec{A} - \vec{\nabla}\chi \quad (1.6)$$

$$\phi' = \phi - \frac{1}{c}\frac{\partial\chi}{\partial t} \quad (1.7)$$

where  $\chi$  is known as the gauge function. Transforming  $\vec{A}$  and  $\phi$  does not change the electric and magnetic fields. This transformation of the potentials is called a gauge transformation and the invariance of the fields and hence Maxwell's equations under such a transformation is called gauge invariance.

The Schrödinger equation for charges in oscillating fields remains invariant under a gauge transformation if the wavefunction transforms as

$$\Psi \Rightarrow e^{i\chi}\Psi \quad (1.8)$$

Depending on the gauge function, we can have multiple solutions for the scalar and vector potentials. Introducing a constraint to this solution to solve for a particular solution is known as gauge condition or gauge fixing. [3],[4] We can set  $\phi = 0$ , which gives us the radiation gauge. Next, we apply the Coulomb gauge:

$$\vec{\nabla} \cdot \vec{A} = 0 \quad (1.9)$$

On replacing  $\vec{p}$  with  $-i\hbar\vec{\nabla}$  in the position representation and applying the radiation gauge, and rewriting the TDSE, we get

$$\left( \frac{1}{2m_e} [i\hbar\vec{\nabla} + \frac{e}{c}\vec{A}(\vec{r}, t)]^2 + V(\vec{r}) \right) \Psi(\vec{r}, t) = i\hbar \frac{\partial\Psi(\vec{r}, t)}{\partial t} \quad (1.10)$$

Applying the Coulomb gauge,

$$-i\hbar[\vec{\nabla} \cdot (\vec{A}\Psi) + \vec{A} \cdot \vec{\nabla}\Psi] = -i\hbar[(\vec{\nabla} \cdot \vec{A})\Psi + \vec{A}(\vec{\nabla} \cdot \Psi) + \vec{A} \cdot \nabla\Psi] = -2i\hbar\vec{A} \cdot \vec{\nabla}\Psi \quad (1.11)$$

the TDSE becomes

$$\left( \frac{1}{2m_e} [-\hbar^2 \nabla^2 - i\hbar \frac{2e}{c} \vec{A}(\vec{r}, t) \cdot \vec{\nabla} + \frac{e^2}{c^2} \vec{A}^2(\vec{r}, t)] + V(\vec{r}) \right) \Psi(\vec{r}, t) = i\hbar \frac{\partial \Psi(\vec{r}, t)}{\partial t} \quad (1.12)$$

This equation contains the semi-classical Hamiltonian which is valid in the strong field regime. An external field is considered strong when its strength is comparable to the strength of the electrostatic field in atoms and molecules. This is discussed in detail in Sections 1.2 and 1.3.

### 1.1.2 Dipole approximation

Another important point to consider in the TDSE is the size of the atom in comparison to the field. As the size of atom is small when compared to the wavelength of the electromagnetic wave,  $\vec{k} \cdot \vec{r} \ll 1$  where  $|\vec{k}| = 2\pi/\lambda$  ( $\lambda$  is the wavelength of the field and  $\langle \vec{r} \rangle$  is the size of the atom). To get an idea of the size of the atom in comparison to the wavelength, let's take  $\lambda = 300$  nm in the ultraviolet region and  $\langle r \rangle = 0.0529$  nm for a hydrogen atom, then,  $\frac{\langle r \rangle}{\lambda} = 1.763 \times 10^{-4}$ . Hence, the expansion of the electric field as Taylor series can be truncated by ignoring the position dependent terms.

$$\vec{E}(\vec{r}, t) = f(t) \vec{E}_0 e^{i(\vec{k} \cdot \vec{r} - \omega t)} \quad (1.13)$$

$$= \vec{E}_0 e^{i\vec{k} \cdot \vec{r}} e^{-i\omega t} \quad (1.14)$$

where  $f(t)$  is the wave envelope term (say,  $\sin^2(t)$ ),  $\omega$  is the frequency of the wave and  $|\vec{E}_0|$  is the amplitude of the wave. Expanding  $e^{i\vec{k} \cdot \vec{r}}$ :

$$\vec{E}(\vec{r}, t) = f(t) \vec{E}_0 \left( 1 + i\vec{k} \cdot \vec{r} - \frac{1}{2!} (\vec{k} \cdot \vec{r})^2 - i \frac{1}{3!} (\vec{k} \cdot \vec{r})^3 + \dots \right) e^{-i\omega t} \quad (1.15)$$

Ignoring the higher order terms which include  $\vec{k} \cdot \vec{r}$  because of the dipole approximation; the time varying electric field can be written as:

$$\vec{E}(t) \approx f(t) \vec{E}_0 e^{-i\omega t} \quad (1.16)$$

The vector potential within the dipole approximation has the form:

$$\vec{A}(t) = -f(t) c \frac{\vec{E}_0}{\omega} i e^{-i\omega t} \quad (1.17)$$

Since the vector potential is independent of  $\vec{r}$  with implications of spatial homogeneity, the magnetic field,  $\vec{B} = 0$ . The TDSE after applying the dipole approximation is now written in what is known as the velocity gauge as:

$$\left( \frac{1}{2m} [-\hbar^2 \nabla^2 - i\hbar \frac{2e}{c} \vec{A}(t) \cdot \nabla + \frac{e^2}{c^2} \vec{A}^2(t)] + V(\vec{r}) \right) \Psi(\vec{r}, t) = i\hbar \frac{\partial \Psi(\vec{r}, t)}{\partial t} \quad (1.18)$$

In Chapter 2, a specific form for the above equation is chosen to describe atoms and molecules in the presence of a high intensity radiation. The next section looks at the various physical processes that have been observed under intense laser fields.

## 1.2 Ionization processes in intense fields

The advancement in laser technology has made possible the study of the interaction of atoms and molecules with fields of intensities of the order of  $10^{14}$  W/cm<sup>2</sup> or higher. Some of the interesting phenomena observed under such high intensities include multiphoton ionization, [5] tunnel ionization and barrier suppression ionization.

Multiphoton ionization (MPI), as the name suggests, occurs when more than one photon is absorbed for ionization. This means that transitions which have energy less than  $I_p$  (Ionization potential) are allowed. If the energy of an  $n$ -photon ( $n > 1$ ) absorption exactly equals the  $I_p$ , the process is a MPI whereas if the the number of photons absorbed are greater than the  $I_p$  the process is more specifically known as Above-Threshold ionization (ATI). Generally, ATI requires fields of intensity greater than those required for MPI. [6] Tunnel ionization (TI) is possible at low-frequency, high-intensity fields. The intensity is relatively higher than that required for multiphoton ionization. This becomes clear from the following physics: at high intensities, the potential gets distorted and begins to oscillate with the frequency of the field. For a sufficiently low frequency, the potential oscillates slowly and the electron can tunnel fast enough before the field changes its sign and the barrier no longer remains suppressed. Quantitatively, the Keldysh parameter [7] is used to determine the possibility of the ionization process. The Keldysh parameter,  $\gamma$ , is a ratio of the tunneling time to the time period of the laser field. When  $\gamma \gg 1$ , TI is more likely and when it is greater than or equal to 1, MPI is more likely. When the intensities are further increased, the field suppresses the potential and this leads to barrier-suppression ionization, a phenomenon where the

electron can easily ionize over the barrier.

Another interesting process which occurs is the high-order harmonic generation (HHG) which can be explained using the *three-step model*. In this process, the three main steps are as follows: first, the electrons undergo tunnel ionization under high intensities, then, they accelerate in a free field and finally, they recombine with the parent ion to generate high energy photons. [8], [9] The intensities required for these ionization processes are typically of the order of  $10^{14} - 10^{15} \text{W/cm}^2$ . Surprisingly, when the strength of the electric field is comparable to or higher than the binding electrostatic field of atoms and molecules, there is a possibility of suppression of ionization. This leads to the formation of the Kramers-Henneberger atom, which is discussed in the next section.

### 1.3 The Kramers-Henneberger atom

To get an idea of the intensities required to form the Kramers-Henneberger atom, the intensity ( $I$ ) of a field calculated as

$$I = \frac{1}{2} \nu c \epsilon_0 |\vec{E}_0|^2 = \frac{P}{4\pi r^2} \quad (1.19)$$

where  $\nu$  is the refractive index of the medium,  $c$  is the speed of light,  $\epsilon_0$  is vacuum permittivity,  $|\vec{E}_0|$  is the amplitude of the electric field and  $P$  is the power of the field equals  $3.51 \times 10^{16} \text{ W/cm}^2$  ( $= 1 \text{ a.u.}$ ) for the hydrogen atom. This is calculated for an electric field of amplitude  $E_0 = 5 \times 10^9 \text{ V/cm}$  and atomic radius  $a_0 = 0.0529 \text{ nm}$ . The atom is inseparable from the external field. Such intense external fields can no longer be considered as a perturbation to the system. In order to easily understand the behavior of the electron, we move to the electron's frame of reference and observe the change in the potential. This change of frame of reference is simply a unitary transformation of the wavefunction in Eq. [1.17] and is referred to as the Kramers-Henneberger transformation. [10]

This phenomenon has been referred to as *atomic stabilization* although this can also be used to stabilize molecules atop barriers. Once we move to the electron's frame of reference (also called the accelerating frame), the potential term becomes a time dependent periodic function and can be expanded as a discrete Fourier series. Under high frequencies, the higher order time-dependent potential terms oscillate extremely

fast and can be neglected within something like a rotating wave approximation. The only significant contribution comes from the first term in the series which is a time averaged potential. For a linearly polarized field this time-averaged potential looks like that of a diatomic molecule for the hydrogen atom with the distance between the two wells given by  $2\alpha_0$  where  $\alpha_0 = \frac{eE_0}{m_e\omega^2}$  and  $\omega$  is the angular frequency of the field and  $E_0$  is the maximum amplitude of the field. [11] For a circularly polarized field, the potential and the electronic cloud for hydrogen were observed to form a torus-shaped object with a radius of  $\alpha_0$ . Note that for a circularly polarized field also,  $\alpha_0 = \frac{eE_0}{m_e\omega^2}$ , but here  $E_0 = k\sqrt{\frac{I_0}{2}}$  whereas for a linearly polarized pulse,  $E_0 = k\sqrt{I_0}$ . [12], [13]  $I_0$  is the intensity of the field and  $k$  is a constant. The physical meaning of  $\alpha_0$  is this: it defines the amplitude of oscillation for an electron in a field.

A number of systems apart from the hydrogen atom in linearly and circularly polarized fields, [14], such as multiply charged anions of hydrogen [15], simple diatomic molecules like hydrogen and helium [16], [17] and two electron quantum dots [18] have been studied using this method. Experiments have also shown evidence for the formation of such stable atoms in the presence of a linearly polarized field. [19] – [22]. A detailed analysis of the experiment by Eichmann. *et al* [20] which produced He and Ne atoms with accelerations up to  $10^{15}$  m/s<sup>2</sup> was done by Wei. *et al*. [23] Here, they showed that the KH force played a significant part in the acceleration of He and Ne atoms in intense laser fields. Recently, Richter *et al*. [24] have even found ways to visualize the electronic structure of these *laser-dressed* atoms using photoelectron spectroscopy. The direction of oscillation of the field plays an important role in deciding the behavior of the atoms. In the next section, three major classifications of light based on the direction of the oscillations of the field are discussed.

### 1.3.1 Polarization

Polarization is the process of restricting the direction of the oscillations of light using a polarizer. An unpolarized electric field oscillates randomly in all directions. Depending on the orientation of the polarizer(s) used, we get linearly, circularly or elliptically polarized field.

Fig.(1.1) shows the forms of the real parts of linearly, circularly and elliptically polarized fields. Linearly polarized field has waves oscillating only in one direction (here the  $x$

direction),

$$E_0 \cos(\omega t) \hat{x} \quad (1.20)$$

while circularly polarized field has waves of equal amplitudes oscillating in two directions ( $x$  and  $y$ ) with a phase difference of  $\pm\pi/2$ .

$$E_0(\cos \omega t \hat{x} + \sin \omega t \hat{y}) \quad (1.21)$$

Elliptically polarized field has waves of unequal amplitudes oscillating in two directions ( $x$  and  $y$ ) with a phase difference of  $\pm\pi/2$ .

$$E_{0_1} \cos \omega t \hat{x} + E_{0_2} \sin \omega t \hat{y} \quad (1.22)$$

$E_0$  and  $\omega$  are the amplitude and angular frequency of the field respectively.

In case of the circularly polarized field, the amplitude of the field along the  $x$  and  $y$  direction equals 1 a.u. whereas for the elliptically polarized field, the amplitude along  $x$  axis is 1 a.u. whereas along  $y$  axis, it is 0.1 a.u. In this thesis, we study benzene in a

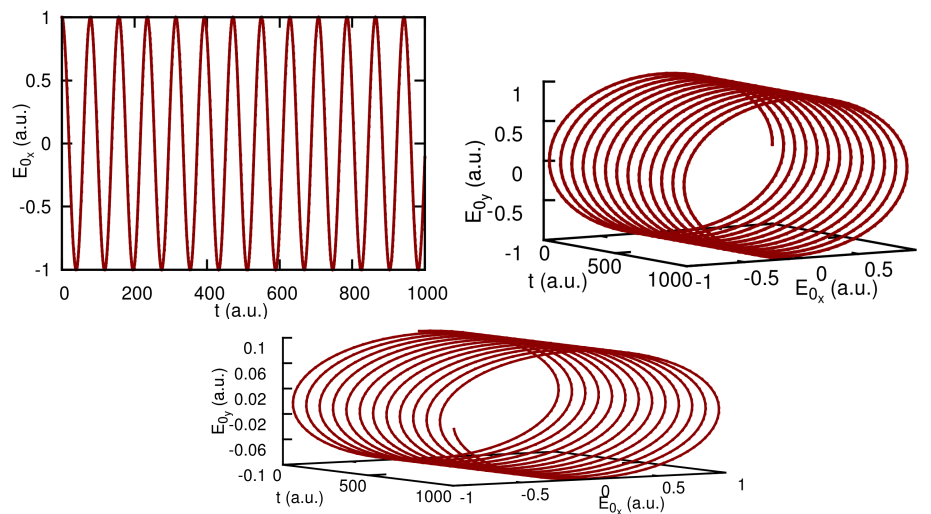


FIGURE 1.1: a) Linearly polarized field  $E_0 \cos(\omega t) \hat{x}$  b) Circularly polarized field along x-y axes  $E_0(\cos \omega t \hat{x} + \sin \omega t \hat{y})$  c) Elliptically polarized field along x-y axes  $E_{0_1} \cos \omega t \hat{x} + E_{0_2} \sin \omega t \hat{y}$ ;  $E_0$  is the amplitude of the field and  $\omega$  is its frequency. The linearly polarized field is seen to oscillate only along the  $x$  axis while the circularly and elliptically polarized fields oscillate along the  $x$  and  $y$  axes with equal amplitudes and unequal amplitudes respectively along both the directions.

circularly polarized pulse. The next section looks at the electronic structure of benzene in the absence of an intense field.

## 1.4 Electronic structure of benzene

Benzene has always been an interesting system to study owing to its aromaticity; it is a planar, ring shaped structure which has a delocalized  $\pi$  electron ring above and below its plane. This  $\pi$ -electron cloud above and below the ring is of importance when it comes to understanding the reactions of benzene since they occupy the valence orbitals. The Hückel molecular orbital (HMO) theory helps us calculate the energies of  $\pi$  MOs of conjugated systems. [25] A conjugated  $\pi$  system has atoms connected to each other via overlapping  $p$  orbitals. Such a system allows for delocalization of electrons, the electrons are not limited to one atom, they belong to all the atoms in the conjugated system. This is based on the following assumptions: [26]

- 1) MOs are constructed as a linear combination of the atomic orbitals (AOs). The electron correlation between  $\sigma$  and  $\pi$  electrons is ignored due to the  $\sigma$  -  $\pi$  orthogonality in planar systems. Only the  $\pi$  electrons are considered.
- 2) For the atomic labels given by  $i$  and  $j$ , the orbital energy  $H_{ij} = \alpha$  when  $i = j$ ;  $H_{ij} = \beta$  when the  $i$ th atom and  $j$ th atom are connected by a  $\sigma$  bond and,  $H_{ij} = 0$  when the two atoms are not adjacent to each other.
- 3) The overlap of electron density integral  $S_{ij} = 0$  when  $i \neq j$  and 1 when  $i = j$ . In other words, a basis set consisting of  $p$  orbitals is orthonormal.

The  $\pi$  MOs of benzene calculated at the HF level theory using 6-311++g\*\* basis set then look like those shown in Fig.(1.2). In this figure, the lowest three orbitals are the bonding  $\pi$  orbitals which hold six  $\pi$  electrons and the highest three orbitals are the anti-bonding  $\pi$  orbitals. The increase in energy of the orbitals is seen as the number of nodal planes increase. The first MO has 1 nodal plane due to the symmetry of the  $\pi$  orbitals, the second and third MOs have 2 nodal planes each, the next two MOs have 3 nodal planes and the highest energy MO has 4 nodal planes. Further, only those orbitals which have the same number of nodal planes are seen to be degenerate.

Another easy method to draw the energy levels of conjugated systems was given by Frost and Musulin in 1953. [27] According to this method (also known as the *polygon method*), a circle is drawn with radius  $2\beta$ . A polygon is inscribed with its one vertex pointing down. For open chain compounds having  $n$  atoms, we construct a polygon having  $2n + 2$  vertices whereas for ring compounds, we inscribe the ring in the circle. Each vertex represents an atom and is projected horizontally to construct the energy level diagram with the energy at the center taken to be equal to  $\alpha$ . Here,  $\alpha$  and  $\beta$

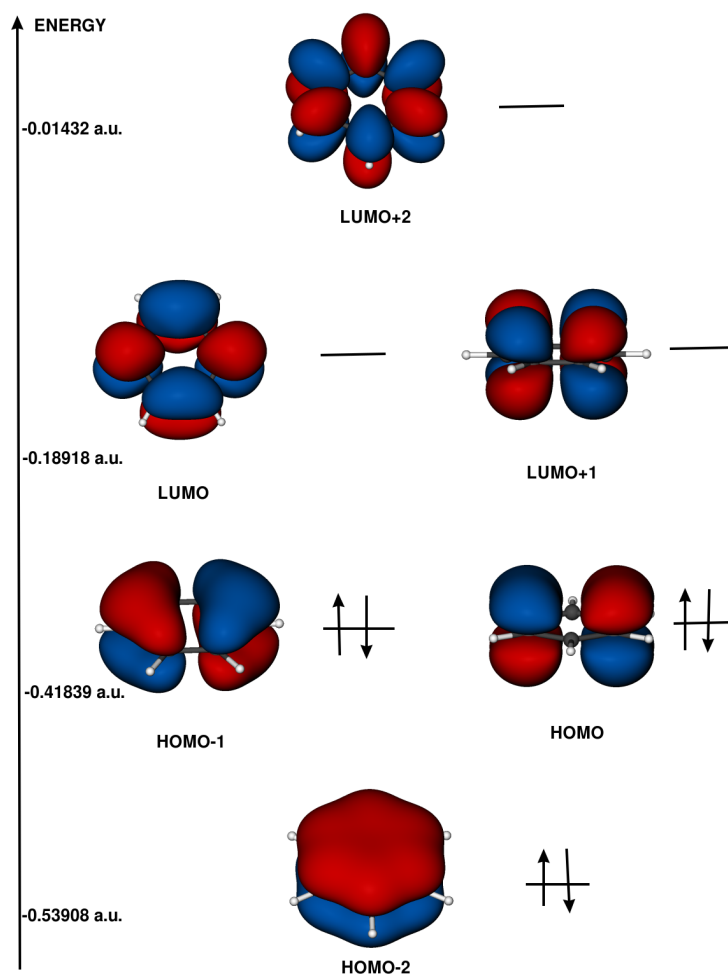


FIGURE 1.2: Hartree-Fock  $\pi$  MOs of benzene calculated using 6-311++g\*\* basis set arranged in an ascending order of energy. The occupancy of these orbitals is depicted schematically using arrows (each arrow represents an electron). The lowest three orbitals are the bonding  $\pi$  orbitals which hold a total of six  $\pi$  electrons. The higher three orbitals are the anti-bonding  $\pi$  orbitals. The energy of the orbitals is seen to increase as the number of nodal planes increase as 1,2,3 and 4. MOs having the same number of nodal planes are degenerate.

have the same meaning as in Hückel theory mentioned above. Fig. (1.3) shows the Frost-Musulin diagram for benzene. Here, the orbitals below the  $\alpha$  energy level are the bonding  $\pi$  orbitals and those above  $\alpha$  are the anti-bonding  $\pi$  orbitals. Although this method does not tell us the values of the orbital energies, one can easily get the energy level diagram of the orbitals and find out the number of degenerate orbitals by looking at the figure.

The photoelectron spectroscopy of benzene shows that the first ionization occurs at 9.2 eV [28] which naturally corresponds to the valence  $\pi$  electrons with  $e_{1g}$  molecular orbital symmetry. Calculations done using 6-311++g\*\* basis set and MP2 level of theory give an  $I_p$  of 9.497 eV. The transition dipole moment calculation for benzene helps us know

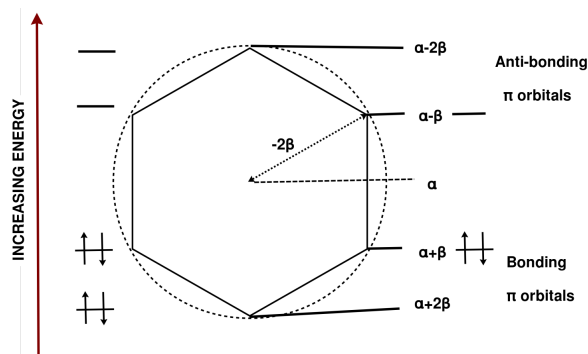


FIGURE 1.3: A graphical representation of the energy levels of benzene using the *polygon method*;  $\alpha$  is the energy of an electron in the  $2p$  orbital and  $\beta$  is the interaction energy between two electrons in two  $2p$  orbitals. (both are conventionally negative). This method easily helps to find out the number of bonding and anti-bonding  $\pi$  orbitals, the energy levels of these orbitals and the number of degenerate orbitals.

which orbitals are involved in the transition and hence which orbitals could be the most affected in the presence of a field. The notations for transitions used below stand for the state symmetry of the molecule. A CIS (Configuration Interaction Singles) calculation for 10 singly excited states of benzene with 100 valence orbitals and 2101 CSFs gives us a significant (and maximum) oscillator strength of 0.952 for the transition from  $A_{1g} \rightarrow B_{1u} + B_{2u} + E_{1u}$ . The  $B_{1u} + B_{2u} + E_{1u}$  state symmetry represents the  $\pi - \pi^*$  transition. These results conform with experimental results in which the electronic spectrum for the absorption of benzene in vapor phase has a band of extremely high intensity near  $1850 \text{ \AA}$  assigned to the  $A_{1g} \rightarrow E_{1u}$  transition, [29] a band of moderate intensity at  $2100 \text{ \AA}$  assigned to the  $A_{1g} \rightarrow B_{1u}$  transition and a weak band at  $2600 \text{ \AA}$  for the  $A_{1g} \rightarrow B_{2u}$  transition. [30] The band at  $2600 \text{ \AA}$  was found to be a vibronic transition. [31] The agreement of the transition dipole moment calculation with the results obtained from symmetry calculations and experiments confirms our choice of the basis set. These calculations on benzene are necessary to understand and compare how the molecular orbitals and the energy levels of these orbitals of benzene change in an intense circularly polarized pulse. In the next section, the reason we have chosen to study benzene becomes clear.

### 1.4.1 Benzene and graphene

Apart from graphene's various applications, its relatively low carrier concentration to metals and its strength make it an ideal material to study field-driven dynamics in conducting materials. [32] Heide. *et al* studied the electron dynamics in graphene in a

strong-field regime (for graphene, this value is only  $2 \times 10^7$  V/m due to its band structure) and observed that they could gain a control over the coherent electron trajectory in graphene. Studies have also been done on HHG in graphene in an elliptically polarized pulse [33] and ionization and HHG in benzene aligned in an intense circularly polarized pulse. [34],[35] HHG on atoms and molecules is being increasingly studied given its application to generate ultrafast laser pulses. Analysis of HHG in graphene suggested that this effect could be extended to more solid-state systems to generate coherent sources of light. Here, we look at the proton transfer through benzene.

Benzene is the basic unit of graphene and can be used as a model to study graphene. Although the electronic structure of both these systems vary, they have delocalized  $\pi$  electrons and are conjugated systems, further, as we will see later, the energy barrier for proton transfer through graphene and benzene and both the systems is comparable. A simple Gaussian calculation done at the MP2 level of theory using 6-311++g\*\* basis set for the proton transfer through benzene gives us a barrier height of 1.63 eV (Fig.1.4) while that for proton transfer through graphene has been calculated to be 1.41 eV. [36] On the left and right sides of the plot in Fig.(1.4) the proton is above and below the

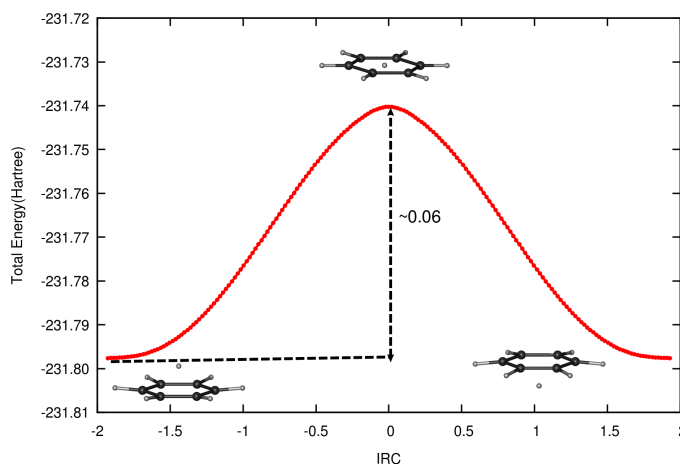


FIGURE 1.4: Energy curve for proton transfer through benzene using the 6-311++g\*\* basis set and MP2 level of theory. This curve was obtained by using Gaussian09 for 401 points. A barrier is seen when the proton sits right at the center of benzene and a minimum is obtained when the proton is exactly above and below benzene respectively.

plane of the benzene molecule respectively. These regions correspond to the minimum in the curve. As the proton moves to the center of benzene, the energy increases and reaches a maximum when the proton lies exactly in the center of the molecule.

## 1.5 Thesis outline

The idea of this work is to look at the behavior of benzene in a high-intensity high-frequency circularly polarized laser pulse. Atoms in an intense circularly polarized pulse show an interesting potential transformation from a single deep potential well to a “doughnut” like potential. Given the  $D_{6h}$  symmetry of benzene, we could expect fascinating results from its potential. In benzene, the electron density in the absence of a field is mainly centered around the carbon atoms. In the presence of an intense field, this density is seen to shift from the edges and above the plane towards the center of the ring. One of the interesting applications of this observation is this; the proton could be held at the center as long as the pulse is on and could be made to move away from the ring by switching off the laser. In other words, we could gain a temporal control over this phenomenon. The effect of circularly polarized pulse on atoms makes not only benzene but any closed molecule having  $\pi$  electrons an interesting system to study.

The first part of the thesis, Chapter 2, deals with the theoretical background required to calculate laser-dressed potentials, the methodology and the basis set required to calculate the KH states. We also look at the potentials for a model system and the hydrogen atom. Further, to check the type of basis set required, energy calculations were done on helium and carbon. In Chapter 3, we observe the KH potential and states of the benzene molecule and its energies at various  $\alpha_0$  values in an intense circularly polarized laser pulse. We discuss and analyze the calculations and results for benzene.

# References

- [1] M. Fox, *Quantum Optics: An introduction*, Oxford University Press
- [2] D. J. Griffiths, *Introduction to Electrodynamics*, Third Edition
- [3] A. D. Bandrauk, F. Fillion-Gourdeau, E. Lorin, *J. Phys. B: At., Mol. Opt. Phys.*, arXiv:1302.2932
- [4] Kuo-Ho Yang, *Am. J. Phys.*, **73**, 742 (2005)
- [5] G. S. Voronov, N. B. Delone, *JETP Letters*, **1**, 66 (1965)
- [6] M. Gavrila, *J. Phys. B: At., Mol. Opt. Phys.*, **35**, 147 (2003)
- [7] L. V. Keldysh, *Soviet Physics JETP*, **20**, 1307 (1964)
- [8] P. B. Corkum, *Phys. Rev. Lett.*, **71**, 1994 (1993)
- [9] K. Kulander, K. Schafer, J. Krause, *Super-Intense Laser-Atom Physics*, **316**, edited by B. Piraux, A. LHuillier and K. Rzazewski (Plenum, New York, 1993)
- [10] W. C. Henneberger, *Phys. Rev. Lett.*, **21**, 838 (1968)
- [11] M. Pont, N. R. Walet, M. Gavrila, C. W. McCurdy, *Phys. Rev. Lett.*, **61**, 939 (1988)
- [12] M. Pont, *Phys. Rev. A*, **40**, 5659 (1989)
- [13] M. Boca, H. G. Mueller, M. Gavrila, *J. Phys. B: At., Mol. Opt. Phys.*, **37**, 147 (2004)
- [14] M. Pont, M. J. Offerhaus, M. Gavrila, *Z Phys D - Atoms, Molecules and Clusters*, **9**, 297 (1988)
- [15] E. Van Duijin, M. Gavrila, H. G. Muller, *Phys. Rev. Lett.*, **77**, 3759 (1996)

- [16] Q. Wei, S. Kais, D. Herschbach, *J. Chem. Phys.*, **129**, 214110 (2008)
- [17] T. Yasuike, K. Someda, *J. Phys. B: At., Mol. Opt. Phys.*, **37**, 3149, (2004)
- [18] P. Raj, P. Balanarayan, *Phys. Chem. Chem. Phys.*, **27**, 297 (2019)
- [19] M. P. de Boer, J. H. Hoogenraad, R. B. Vrijen , R. C. Constantinescu , L. D. Noordam, H. G. Muller, *Phys. Rev. A*, **50**, 4085 (1994)
- [20] U. Eichmann, T. Nubbemeyer, H. Rottke, W. Sandner, *Nature*, **461**, 1261 (2009)
- [21] U. Eichmann, H. Zimmermann, S. Eilzer, *Phys. Rev. Lett.*, **112**, 113001 (2014)
- [22] U. Eichmann, H. Zimmermann, S. Eilzer, *J. Phys. B: At., Mol. Opt. Phys.*, **47**, 204014 (2014)
- [23] Q. Wei, P. Wang, S. Kais, D. Herschbach, *Chem. Phys. Lett.*, **683**, 240 (2017)
- [24] F. Morales, M. Richter, S. Patchovskii, O. Smirnova, *PNAS*, **108**, 16906 (2011)
- [25] E. Hückel, *Z. Physik*, **70**, 204 (1931)
- [26] W. Kutzelnigg, *J. Comput. Chem.*, **28**, 25 (2007)
- [27] A. A. Frost, B. Musulin, *J. Chem. Phys.*, **20**, 572 (1953)
- [28] A. W. Potts, W. C. Price, D. G. Streets, T. A. Williams, *Faraday Discuss. Chem. Soc.*, **54**, 168 (1972)
- [29] H. Sponer, G. Nordheim, A. L. Sklar, E. Teller, *J. Chem. Phys.*, **7**, 207 (1939)
- [30] W. C. Price, A. D. Walsh, *Proc. Roy. Soc.*, **A191**, 22 (1947)
- [31] G. H. Atkinson, C. S. Parmenter, *J. Mol. Spec.*, **73**, 31 (1978)
- [32] C. Heide, T. Higuchi, H. B. Weber, P. Hommelhoff, *Phys. Rev. Lett.*, **121**, 207401 (2018)
- [33] N. Yoshikawa, T. Tamaya, K. Tanaka, *Science*, **356**, 736 (2017)
- [34] P. Zdanska, V. Averbukh, *J. Chem. Phys.*, **118**, 8726 (2003)
- [35] R. Baer, D. Neuhauser, P. Zdanska, N. Moiseyev, *Phys. Rev. A*, **68**, 043406 (2003)
- [36] M. Miao, M. Buongiorno Nardelli, Qi Wang, Yingchun Liu , *Phys. Chem. Chem. Phys.*, **15**, 16132 (2013)

## Chapter 2

# Kramers-Henneberger potentials, states of model and atomic systems in a circularly polarized pulse

In this chapter, in the first section, we look at the derivation of the KH time-averaged potential for atoms in a circularly polarized pulse. In the next section, we look at the KH potentials for a model system and hydrogen. Finally, we explain the choice of an even tempered Gaussian basis set to describe the KH states since in the case of KH states in a circularly polarized pulse, a standard Gaussian basis set is not good enough. Helium and carbon were used as test cases to verify the choice of the basis set.

### 2.1 Kramers-Henneberger transformation

The KH transformation is a unitary transformation from the laboratory frame to the oscillating frame or the KH frame of reference. In the laboratory frame, the electron oscillates as a function of the laser parameters whereas in the KH frame, it is the Coulomb potential that oscillates. The time-averaged part of this potential is what we call the

zeroth order KH potential. This transformation is done as follows:

$$\Psi = \hat{\Omega}\psi \quad (2.1)$$

where  $\hat{\Omega}$  is given by

$$\hat{\Omega} = \exp\left[\frac{i}{\hbar}\int_{-\infty}^t\left(\frac{e}{m_e c}\vec{A}(\tau)\cdot\nabla + \frac{e^2}{2m_e c^2}\vec{A}^2(\tau)d\tau\right)\right] \quad (2.2)$$

Replacing  $\Psi$  with  $\hat{\Omega}\psi$  converts the Schrödinger equation in the velocity gauge (Eq. [1.17]) into a very familiar form

$$i\hbar\frac{\partial\psi}{\partial t} = [\hat{\Omega}\hat{H}\hat{\Omega}^\dagger - i\hbar\hat{\Omega}\frac{\partial\hat{\Omega}^\dagger}{\partial t}]\psi \quad (2.3)$$

The Baker-Campbell-Hausdorff [1] formula is used to evaluate  $\hat{\Omega}\hat{H}\hat{\Omega}^\dagger$  for every term in the Hamiltonian  $\hat{H}$ . The formula is as follows:

$$e^{[Y]}\hat{X}e^{-[Y]} = \hat{X} + [Y, \hat{X}] + \frac{1}{2!}[Y, [Y, \hat{X}]] + \dots \quad (2.4)$$

The time dependent terms in the Hamiltonian commute with  $\hat{\Omega}$  and cancel out the  $-i\hbar\hat{\Omega}\frac{\partial\hat{\Omega}^\dagger}{\partial t}$  term. Since the kinetic energy term also commutes with  $\hat{\Omega}$ , we are left with  $e^{\hat{\Omega}_1}V(\vec{r})e^{-\hat{\Omega}_1}$  where

$$\hat{\Omega}_1 = \frac{i}{\hbar}\int_{-\infty}^t\frac{e}{m_e c}\vec{A}(\tau)\cdot\nabla d\tau \quad (2.5)$$

Using the same formula as above, we get

$$V(\vec{r}) + [\hat{\Omega}_1, V(\vec{r})] + \frac{1}{2!}[\hat{\Omega}_1, [\hat{\Omega}_1, V(\vec{r})]] + \dots = V(\vec{r}) + (\vec{\alpha}\cdot\nabla)V(\vec{r}) + \frac{1}{2!}(\vec{\alpha}\cdot\nabla)^2V(\vec{r}) + \dots \quad (2.6)$$

where

$$\vec{\alpha}(t) = -\int_{-\infty}^t\frac{e}{m_e c}d\tau\vec{A}(\tau) \quad (2.7)$$

$$\Rightarrow \vec{\alpha}(t) = \frac{-e}{m_e c}\frac{d\vec{A}(t)}{dt} = \frac{e}{m_e}\vec{E}(t) = \frac{e}{m_e}\vec{E}_0\cos\omega t \quad (2.8)$$

$$\Rightarrow \vec{\alpha}(t) = \frac{e\vec{E}_0}{m_e\omega^2}\cos\omega t = \vec{\alpha}_0\cos\omega t \quad (2.9)$$

for a linearly polarized light. In our case, since we consider a circularly polarized light in the x-y plane, the electric field and  $\vec{\alpha}$  are given as

$$\vec{E}_0(t) = E_0\hat{x} + E_0^{i\frac{\pm\pi}{2}}\hat{y} + 0\hat{z} \quad (2.10)$$

$$\Rightarrow \vec{E}(t) = E_0e^{(-i\omega t)}(\hat{x} \pm i\hat{y}) \quad (2.11)$$

$$\Rightarrow \text{Re}[\vec{E}(t)] = E_0(\cos\omega t\hat{x} \mp \sin\omega t\hat{y}) \quad (2.12)$$

$$\Rightarrow \vec{\alpha}(t) = \alpha_0(\cos\omega t\hat{x} \mp \sin\omega t\hat{y}) \quad (2.13)$$

The evaluation for the potential term gives a Taylor expansion of  $V(\vec{r})$  about  $\vec{r}$  which translates the potential by  $\vec{\alpha}$ . The Schrödinger equation can be now written as

$$i\hbar\frac{\partial\psi(\vec{r},t)}{\partial t} = \frac{1}{2m_e}[-\hbar^2\nabla^2 + V(\vec{r} + \vec{\alpha}(t))]\psi(\vec{r},t) \quad (2.14)$$

$V(\vec{r} + \vec{\alpha}(t))$  is called the Kramers-Henneberger potential and is a periodic function. Since we have only done the time-independent calculations here, it is more accurate to write the Time-Independent Schrödinger equation (TISE),

$$\frac{1}{2m_e}[-\hbar^2\nabla^2 + V(\vec{r} + \vec{\alpha}(t))]\psi(\vec{r}) = E^{KH}\psi(\vec{r}) \quad (2.15)$$

For molecules, we include the electronic and nuclear repulsion terms which gives us,

$$\left[ \sum_i \frac{-\hbar^2}{2m_e} \nabla_e^2 + \sum_{i,A} V_{Ne}(\vec{r}_{iA} + \vec{\alpha}(t)) + \sum_{i,j} V_{ee}(\vec{r}_{ij}) + \sum_{A,B} V_{NN}(\vec{r}_{AB}) \right] \psi(\vec{r}) = E^{KH} \psi(\vec{r}) \quad (2.16)$$

### 2.1.1 Kramers-Henneberger potential

Since the potential is periodic with  $T = \frac{2\pi}{\omega}$ , it can be expanded in a discrete Fourier series as [2]

$$V^{KH}(\vec{r} + \vec{\alpha}(t)) = V_0^{KH}(\vec{r}) + \sum_{n=1}^{\infty} V_n^{KH}(\vec{r}) \cos(n\omega t) \quad (2.17)$$

$$V_n^{KH}(\vec{r}) = \frac{1}{T} \int_0^T V^{KH}(\vec{r} + \vec{\alpha}(t)) \cos(n\omega t) dt \quad (2.18)$$

The harmonics (except  $n = 0$ ) under high frequencies, show extremely fast oscillations and can be averaged to zero. We are then left with the zeroth order term in the series

which is a time-averaged stabilizing potential and is known as the zeroth order Kramers-Henneberger potential. The zeroth order potential can be written as

$$V_0^{KH} = \frac{1}{T} \int_0^T V(\vec{r} + \vec{\alpha}(t)) dt \quad (2.19)$$

For the model potential,

$$V(x, y) = -0.63 \exp[-0.1424(x^2 + y^2)] \quad (2.20)$$

the KH potential is,

$$V^{KH}(\vec{r} + \vec{\alpha}(t)) = -0.63 \exp[-0.1424(x - \alpha_0 \cos(\omega t))^2 + y - \alpha_0 \sin(\omega t)^2] \quad (2.21)$$

Similarly, for the hydrogen atom  $V(\vec{r}) = \frac{-1}{|\vec{r}|}$ , the KH potential is:

$$V^{KH}(\vec{r} + \vec{\alpha}(t)) = \frac{-1}{\sqrt{(x - \alpha_0 \cos(\omega t))^2 + (y - \alpha_0 \sin(\omega t))^2 + z^2}} \quad (2.22)$$

For benzene, the potential  $V(\vec{r}, \vec{R}) = \sum_{i,A} -Z_A/|\vec{r}_i - \vec{R}_A|$  where  $\vec{r}_i$  and  $\vec{R}_A$  are the position vectors of the electrons and nuclei respectively transforms as:

$$V^{KH}(\vec{r} + \vec{\alpha}(t)) = \sum_{i,A} \frac{-Z_A}{\sqrt{(x_i - \alpha_0 \cos(\omega t) - x_A)^2 + (y_i - \alpha_0 \sin(\omega t) - y_A)^2 + (z_i - z_A)^2}} \quad (2.23)$$

## 2.2 Model potential and hydrogen atom

Kramers-Henneberger time independent potential and the higher order harmonics were calculated for the model potential. Fig.(2.1) shows the 2D contours for the zeroth order potential and the harmonics for  $n = 1$  to 5. The zeroth order potential oscillates with the pulse in a circular fashion and so if we consider the time averaged potential, it comes out to be in the shape of a ring whose radius equals  $\alpha_0$ . For the higher order harmonics, nodal planes increase as  $n$  increases. The number of nodal planes are equal to  $n - 1$  for the  $n$ th term in the potential. As  $n$  increases, the magnitude of the higher order potential terms are very small compared to the zeroth order term. These potentials were calculated according to the Eq. [2.18], where  $V^{KH}$  for the model system and hydrogen

are given by Eq. [2.21] and Eq. [2.22] respectively. Just as in the case of the  $V_0^{KH}$  for

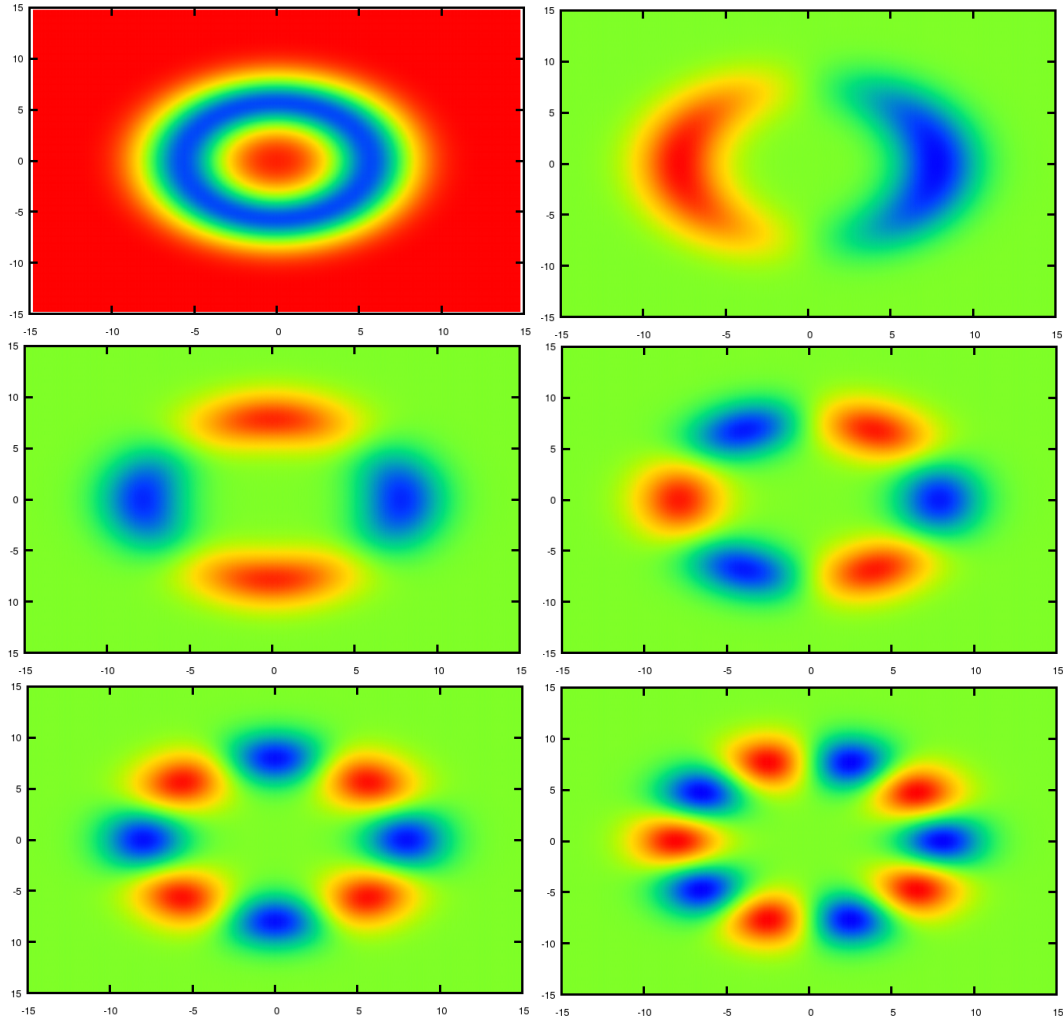


FIGURE 2.1: Contours of  $V_n^{KH}(\vec{r})$  for the model potential  $n=0-5$  calculated (according to Eq. [2.18]).  $V_0^{KH}$  contour is a circle with zero nodes. As  $n$  increases, the number of nodal planes increase as  $n-1$ . Red and blue stand for positive and negative potential values respectively.

the model system in Fig.(2.2), hydrogen atom also has a ring like or “doughnut” shaped zeroth order potential. The potential also looks similar to a torus of a radius  $r$  and center  $c$ , whose equation in Cartesian coordinates is given by:

$$r^2 = (c - \sqrt{x^2 + y^2 + z^2})^2 \quad (2.24)$$

Carbon atom shows the same potential qualitatively but has a deeper potential. This is expected since carbon has a greater number of electrons than hydrogen, the potential has to hold more bound states of the atom. The higher order harmonics for hydrogen and carbon average to zero for high frequencies, in the ultraviolet range, and can be neglected.

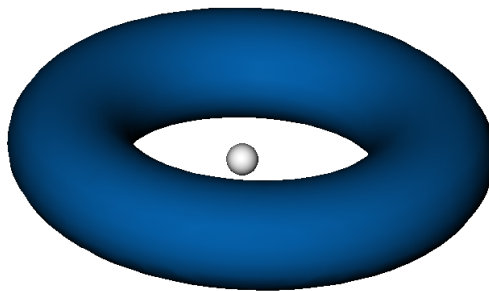


FIGURE 2.2: The isosurface of  $V_0^{KH}$  for hydrogen at an isovalue = -3.7207 a.u. visualized using VMD. [3] The potential oscillates in a circular motion to give a ring shaped time-averaged potential. The ring like structure implies there is no potential at the center for this isovalue.

Throughout this work, red represents a positive isovalue and dark blue represents a negative isovalue.

## 2.3 Methodology

The flow-chart for the methodology [4], [5] has been given in Fig.(2.3). It is explained below.

To calculate the KH potential : We generated a grid for the Gauss-Legendre integration. The nuclear-electron transformed potentials ( $V^{KH}(\vec{r} + \vec{\alpha}(t))$ ) were calculated at these grid points using GAMESS. [6],[7] These potentials were then averaged by  $2\pi$  to give the KH potential.

To calculate the KH states: The TISE was solved by feeding the KH potential into GAMESS. The kinetic energy terms and the two-electron repulsion terms in the Hamiltonian do not change. HF energies and CIS state energies were calculated from GAMESS. For benzene, the number of valence orbitals for the CIS calculation were taken to be 100 and the number of CSFs were 2101. In order to perform calculations for the KH states, a modified basis set which included the even-tempered Gaussian series was considered. This is discussed in the next section.

## 2.4 Even-tempered Gaussian basis set

The KH potentials for the model potential and hydrogen atom clearly tell us that the KH states which the potential holds will be centered on the ring. The orbitals can be

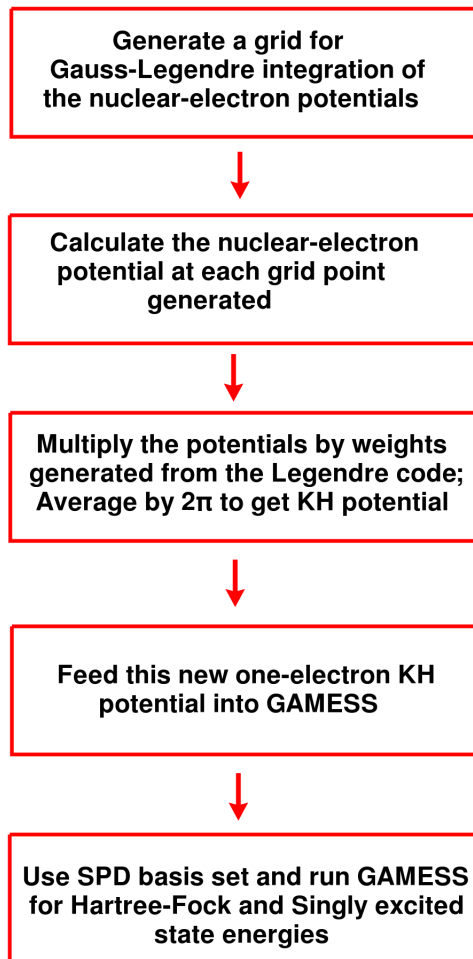


FIGURE 2.3: A flow chart explaining the steps to calculate the KH potentials and energies.

thought to look similar to the  $d_z^2$  Gaussian function,

$$\frac{1}{2}\beta^{\frac{7}{4}}\exp(-\beta r^2)[2z^2 - x^2 - y^2] \quad (2.25)$$

In order to account for these orbitals, we would have to incorporate a significant number of D shells in the basis set. For the helium atom, an SPD type basis was constructed where the S and P shells were taken from the coemd-ref [8] basis set but their number was modified to include more D shells. The exponents of the Gaussian primitives for the D shells were taken as a geometric progression with common ratio 2 (see Appendix A). These are known as an even-tempered Gaussians (ETG). It was proven empirically by Schmidt and Ruedenberg [9] that using a large number of Gaussian primitives for an even-tempered Gaussian series gives accurate SCF (Self-consistent field) energies.

## 2.5 KH states of helium

The occupied orbital of helium was observed as  $\alpha_0$  was varied for this fixed basis set.

We can see from Fig.(2.4) that using the SPD-type basis set gives an s-type orbital

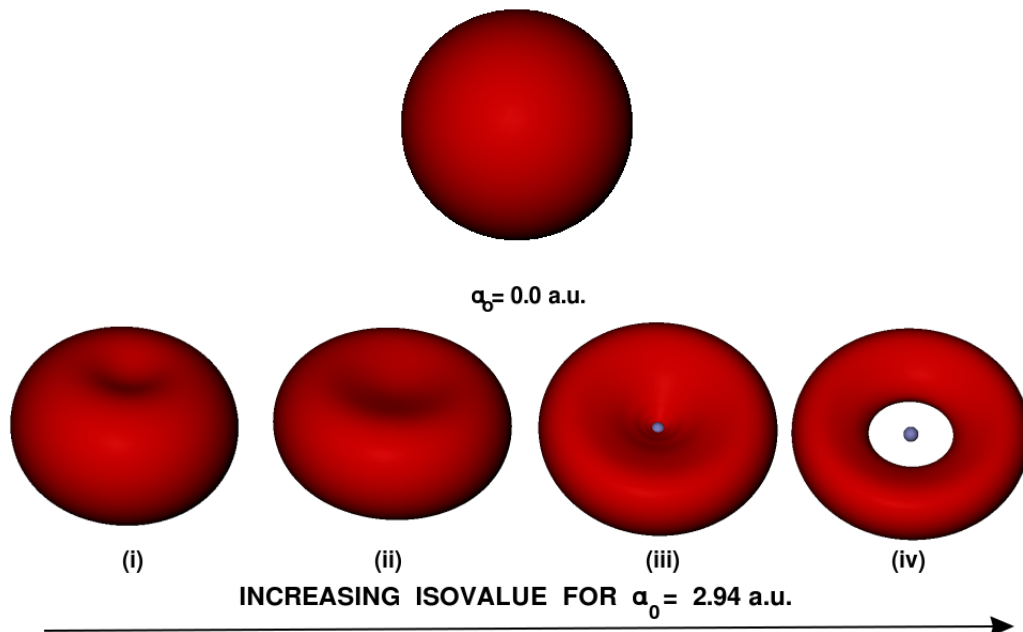


FIGURE 2.4: Helium  $1s$  Hartree-Fock orbital at  $\alpha_0 = 0.0$  a.u. and the ring shaped KH orbital at  $\alpha_0 = 2.94$  a.u. at isovalues (i) 0.008782, (ii) 0.022298, (iii) 0.029056 and (iv) 0.030454 calculated using the SPD-type basis set. From the lowest isovalue itself, we see a dip in the center of the orbital. The second isovalue shows an elongation of the orbital. For the third isovalue, we can see the ring begins to show and the ring is clearly seen for the maximum isovalue.

for  $\alpha_0 = 0.0$  a.u. similar to any standard Gaussian basis set. The energy of helium using this basis set was found to be  $-2.9021$  a.u. This value differs slightly from the energy obtained using coemd-ref which is  $-2.8616$  a.u. When we increase the  $\alpha_0$  value, the orbital looks similar to the potential obtained for the model system and hydrogen. Fig.(2.5) shows the variation of KH Hartree-Fock energies with  $\alpha_0$ . A sharp increase in energy is seen up to  $\alpha_0 > 1$  with a discontinuity at  $\alpha_0 = 1$ . This could be due to an insufficient number of basis set functions. Although, an increase in energy is observed beyond this value, it is comparatively much slower than the rise for  $\alpha_0 > 1$ .

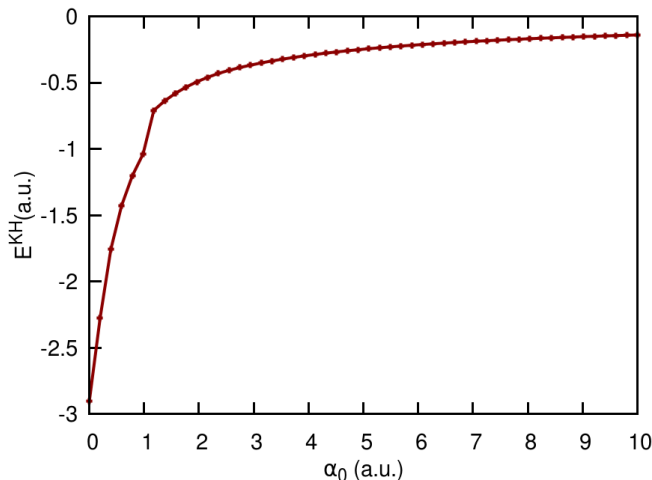


FIGURE 2.5: The Hartree-Fock KH energies ( $E^{KH}$ ) (a.u.) of the KH states of helium with varying  $\alpha_0$ . The basis set used was the SPD-type basis set given in Appendix A. The ground state energy at  $\alpha_0 = 0$  is -2.90212 a.u. The rise in energy is sharp for  $\alpha_0 > 1$ . At 1, there is a discontinuity in the plot which could have occurred due to the basis. Beyond 1, the rise in energy is comparatively slow.

## 2.6 KH states of carbon

Similar calculations were done for carbon. The S and P shells were taken from the coemd-ref basis set for carbon but the D shell exponents were kept constant. Fig.(2.6) shows only the occupied orbitals for the carbon atom at  $\alpha_0 = 0.0$  a.u. and at  $\alpha_0 = 3.0$  a.u. At  $\alpha_0 = 0.0$  a.u., the orbitals are the free-field  $1s$ ,  $2s$  and  $2p$  atomic orbitals. The  $1s$  orbital looks like a ring at  $\alpha_0 = 3.0$  a.u. and the  $2s$  and  $2p$  orbitals break down to form  $d$  type orbitals. We can see that these orbitals are degenerate with an equal energy of -0.1580 a.u. and contain two nodal planes each. This trend was observed in carbon for all values of  $\alpha_0 \neq 0$  that we considered. Fig.(2.7) shows the plot for Hartree-Fock KH energies of carbon vs  $\alpha_0$ . Here, again there is a sharp increase in energy for a small  $\alpha_0$  value and then a gradual increase as  $\alpha_0$  further increases.

In the next chapter, we look at the calculations for benzene in a circularly polarized pulse using this basis set.

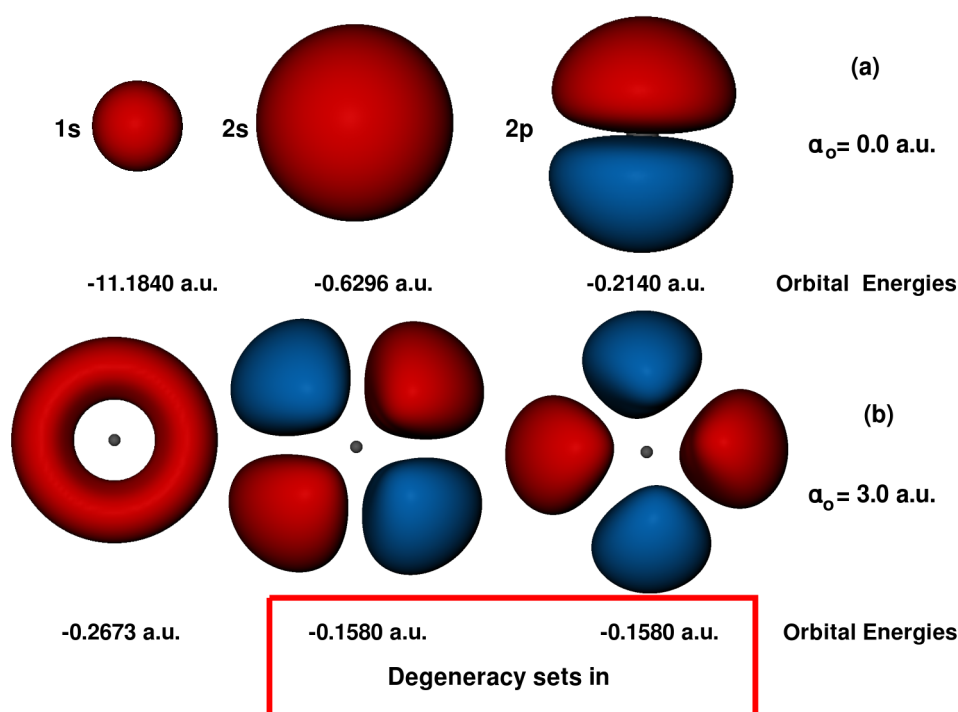


FIGURE 2.6: Occupied orbitals of the carbon atom at a)  $\alpha_0 = 0.0$  a.u. and b)  $\alpha_0 = 3.0$  a.u. calculated using the SPD-type basis set at the Hartree-Fock level of theory. As  $\alpha_0$  increases, the core  $1s$  orbital goes from a sphere to a “doughnut” shape and the  $2s$  and  $2p$  orbitals no longer exist; we instead get  $d$  type degenerate orbitals with two nodal planes each.

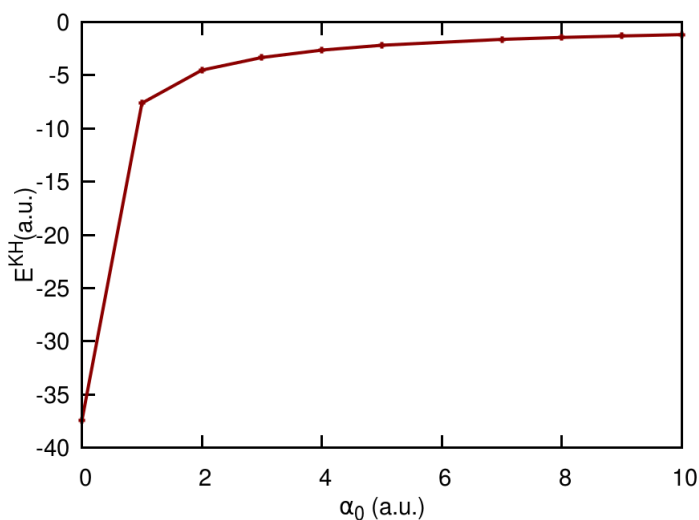


FIGURE 2.7: Hartree-Fock KH energies calculated for 10  $\alpha_0$  values for the carbon atom. The ground state energy at  $\alpha_0$  is -37.422 a.u. Similar to helium, the energy initially shows a sharp increase in energy for  $\alpha_0$  up to 1 a.u. and then gradually increases.

# References

- [1] G.B. Arfken, H.J. Weber, F.E. Harris, *Mathematical Methods for Physicists*, 7th Edition, Elsevier (2013)
- [2] Ido Gillary, N. Moiseyev, *Phys. Rev. A*, **66**, 063415 (2002)
- [3] W. Humphrey, A. Dalke, K. Schulten, *J. Molec. Graphics*, **14**, 33 (1996)
- [4] P. Balanarayan, N. Moiseyev, *Mol. Phys.*, **111**, 1814 (2013)
- [5] P. Raj, P. Balanarayan, *Phys. Chem. Chem. Phys.*, **27**, 297 (2019)
- [6] M.W. Schmidt, K.K. Baldridge, J.A. Boatz, S.T. Elbert, M.S. Gordon, J.H. Jensen, S. Koseki, N. Matsunaga, K.A. Nguyen, S.Su, T.L. Windus, M. Dupuis, J.A. Montgomery, *J. Comput. Chem.*, **14**, 1347 (1993)
- [7] M.S. Gordon, M.W. Schmidt and C.E. Dykstra, G. Frenking, K.S. Kim, G.E. Scuseria (editors), *Advances in electronic structure theory: GAMESS a decade later in Theory and Applications of Computational Chemistry: the first forty years*, Elsevier, 1167 (2005)
- [8] J. Lehtola, P. Manninen, M. Hakala and K. Hmlinen, *J. Chem. Phys.*, **137**, 104105 (2012).
- [9] M.W. Schmidt, K. Ruedenberg, *J. Chem. Phys.*, **71**, 3951 (1979)

## Chapter 3

# Benzene in a circularly polarized pulse

### 3.1 Kramers-Henneberger potential of benzene

In the previous chapter, we saw that a single atom shows a ring like potential in the presence of a circularly polarized pulse. The radii of these potentials increase with increasing  $\alpha_0$ . If six such potentials are considered for six carbon atoms in benzene, they begin to intersect each other when the  $\alpha_0$  is greater than half the C-C bond distance. We see in the schematic Fig.(3.1) below that when the  $\alpha_0$  value equals the C-C bond distance, all the potentials intersect in the center. It is important to note here that the plane of the circularly polarized pulse has to be in the plane of the molecule. If the pulse was perpendicular to the plane of benzene, the potentials would also form a ring perpendicular to the plane. This would not give us the desired results as there would be no intersection of the potentials. In the schematic, we don't consider the intersection of potentials due to hydrogen atoms. This is because hydrogen atoms only contribute 6 electrons in benzene compared to 36 electrons from the carbon atoms. Hence, it is safe to say that the potential in the center majorly holds the bound states of the electrons from the carbon atoms.

The contributions of the higher order potential terms are also ignored. The next figure makes this clear. The higher order harmonics were calculated and visualized in VMD for  $\alpha_0 = 2.7$  a.u. (The choice of this  $\alpha_0$  was based on the C-C bond distance of benzene

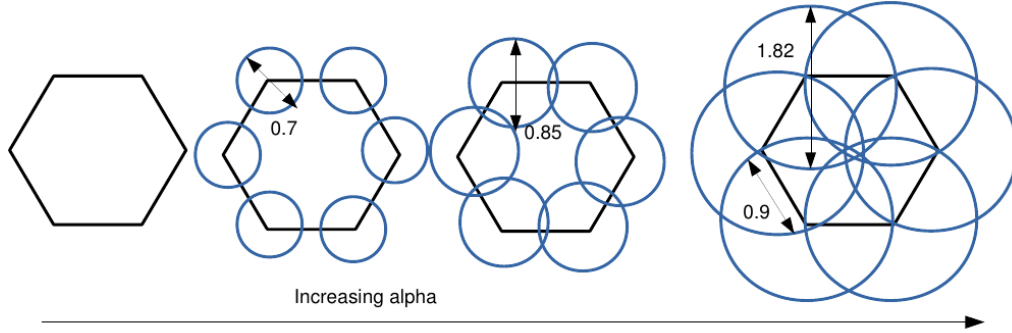


FIGURE 3.1: A schematic diagram showing varying radii of the six circles (potentials) for varying  $\alpha_0$ .  $\alpha_0 = \text{Radius of the circle}$ . The radius of each circle increases on increasing the  $\alpha_0$  value. In the last diagram, we see that the radius of the circle equals the side of the hexagon; this gives an intersection of all the six circles in the center which would give a deep minimum. This means that most of the electrons will be held here.

(2.67 a.u.) These harmonics are calculated according to the equation for higher order Fourier coefficient terms,

$$V_n^{KH}(\vec{r}) = \frac{1}{T} \int_0^T \sum_{i,A} \frac{-Z_A \cos(n\omega t)}{\sqrt{(x_i - \alpha \cos(\omega t) - X_A)^2 + (y_i - \alpha \sin(\omega t) - Y_A)^2 + (z_i - Z_A)^2}} dt \quad (3.1)$$

These potential terms as can be seen from Fig.(3.2) appear symmetric for all the  $n$  values and suggest a possible spatial cancellation. The plots for these potential terms show no value of the potential at the center, hence it can be concluded that the higher order terms do not interfere significantly with the zeroth order KH potential. Further, on increasing  $n$ , the potential is more dispersed due to the increase in the number of nodes. In Fig.(3.3), graphs of  $V_0^{KH}$  for benzene vs  $\alpha_0$  values along the x-y axes show

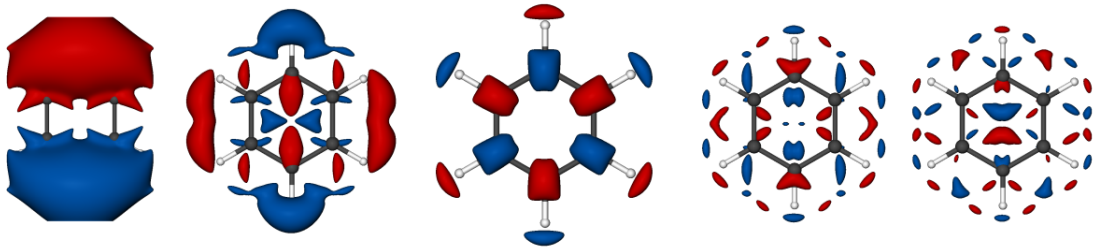


FIGURE 3.2: Isosurfaces of the higher order harmonics of benzene  $V_n^{KH}(\vec{r})$  for  $n = 1-5$  calculated according to the Eq.[3.1]. These potentials were visualized at an isovalue of  $|\pm 1|$ .

us the form of these potentials. This figure looks at the potential values along the x and y axes for three different  $\alpha_0$  values, 2.3 a.u., 2.7 a.u. and 3.0 a.u. Calculations were

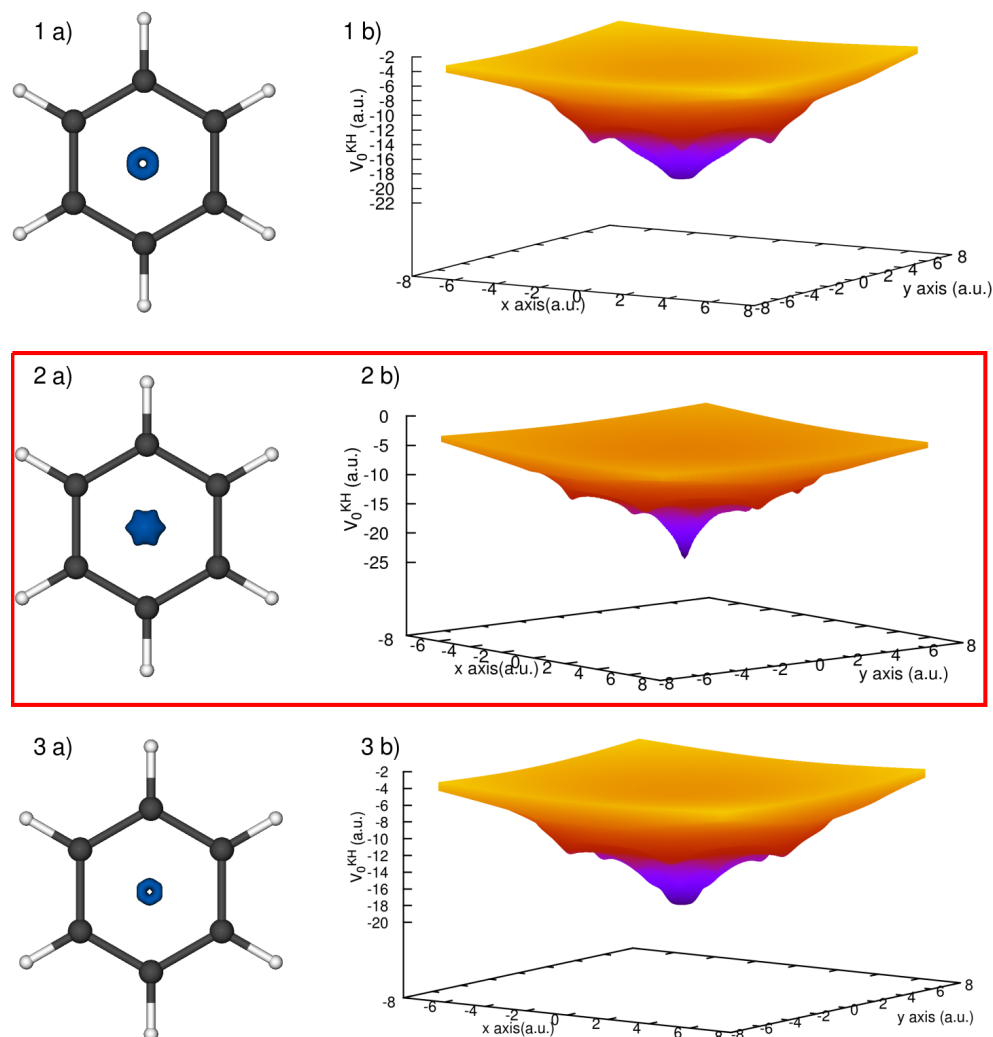


FIGURE 3.3: a) Isosurfaces calculated at isovalues 1a) 19.6 a.u., 2a) -19.8801 a.u. and 3a) 18.4462 a.u. and b) 2D plots of  $V_0^{KH}$  for  $\alpha_0 =$  (1) 2.3 a.u. (2) 2.7 a.u. (3) 3.0 a.u. Visualization of the isosurfaces was done with the help of VMD. The isosurface is maximum at the center at  $\alpha_0 = 2.7$  a.u. (in the red box) close to the C-C bond distance value of 2.67 a.u. As we increase and decrease the  $\alpha_0$  values, the maximum shifts away from the center. The plot of the potential shows the same idea graphically. The local minima in each graph arise due to the intersection of two carbon atoms (can be seen from the schematic diagram).

done at these values since the C-C bond distance obtained from optimizing benzene using GAMESS and the 6-311++g\*\* basis set was found to be 2.67 a.u. The potentials were calculated on a cubic grid and the isosurfaces on the right of the Fig.(3.3) were visualized using VMD. From the graphs of the potentials, we see that the magnitude of the potential is maximum at the center for  $\alpha_0 = 2.7$  a.u. and decreases on increasing or decreasing the  $\alpha_0$  value. As expected, this value is close enough to the C-C bond distance obtained from GAMESS optimization of benzene. The isosurface plot similarly shows that there is a maximum in the center for the same  $\alpha_0$  value. The local minima

which can be seen symmetrically flanked on either side of the global minimum are due to the intersection of two carbon atoms and two hydrogen atoms. These intersections are expected and can be seen in the schematic in Fig.(3.1) The symmetrical nature of these minima is due to the symmetry of the molecule.

### 3.1.1 Kramers-Henneberger states of benzene

In this section, we present all the electronic structure calculations of benzene. Only a partial analysis has been done so far, regarding the orbital energies and the CIS states, although the electronic densities confirm our theory and the correctness of our potential calculations. Fig.(3.4) shows the core molecular orbital along with HOMO-3, HOMO-2, HOMO-1 and HOMO and the total electronic density for the molecule with varying  $\alpha_0$ . The core MO and the electronic density of benzene show a similar trend; at  $\alpha_0 = 0.0$ , the isosurfaces for both are centered on the carbon atoms and as  $\alpha_0$  increases, they shift towards the center. At  $\alpha_0 = 2.7$  a.u., (the same value for which we observed a deep minimum in the KH potential), both the core MO as well as electron density show a maximum at the center. In case of the other MOs, we see the three bonding  $\pi$  orbitals of benzene up to  $\alpha_0 = 1.5$  a.u. although their energy levels are constantly changing. At  $\alpha_0 = 2.7$  a.u. and 3.0 a.u., we no longer see the degenerate  $\pi$  orbitals. Instead, we see the formation of three new orbitals, out of which two still show degeneracy. Although a complete analysis has not been made for these MOs, the electronic density calculations give us the expected results. In order to understand the behavior of the orbitals, Hartree-Fock energy calculations and CIS calculations were done.

The Hartree-Fock energies of benzene with varying  $\alpha_0$  in Fig. (3.5) show a smooth curve with a continuous increase in energy for the SPD-type basis set. It is important to note here that at this basis set, the energy of benzene is seen to be -224.289 Hartree whereas the ground state energy of benzene calculated at the 6-311++g\*\* basis set was found to be -230.745 Hartree. This is an energy difference of almost 6.5 Hartree. This basis set gives us an understanding of the kind of basis functions important for a system in a circularly polarized field and we are yet to arrive at a converged basis set. Again, it can be seen that for small  $\alpha_0 < 0.5$  a.u., the increase in energy is sudden. For  $\alpha_0 > 0.5$  a.u., the increase is comparatively slower and tends to 0 as  $\alpha_0$  goes to 3.5 a.u.

Fig.(3.6) looks at the Hartree-Fock molecular orbital energies as a function of  $\alpha_0$ . The core six MOs show a significant change in energy as  $\alpha_0$  varies as compared to the

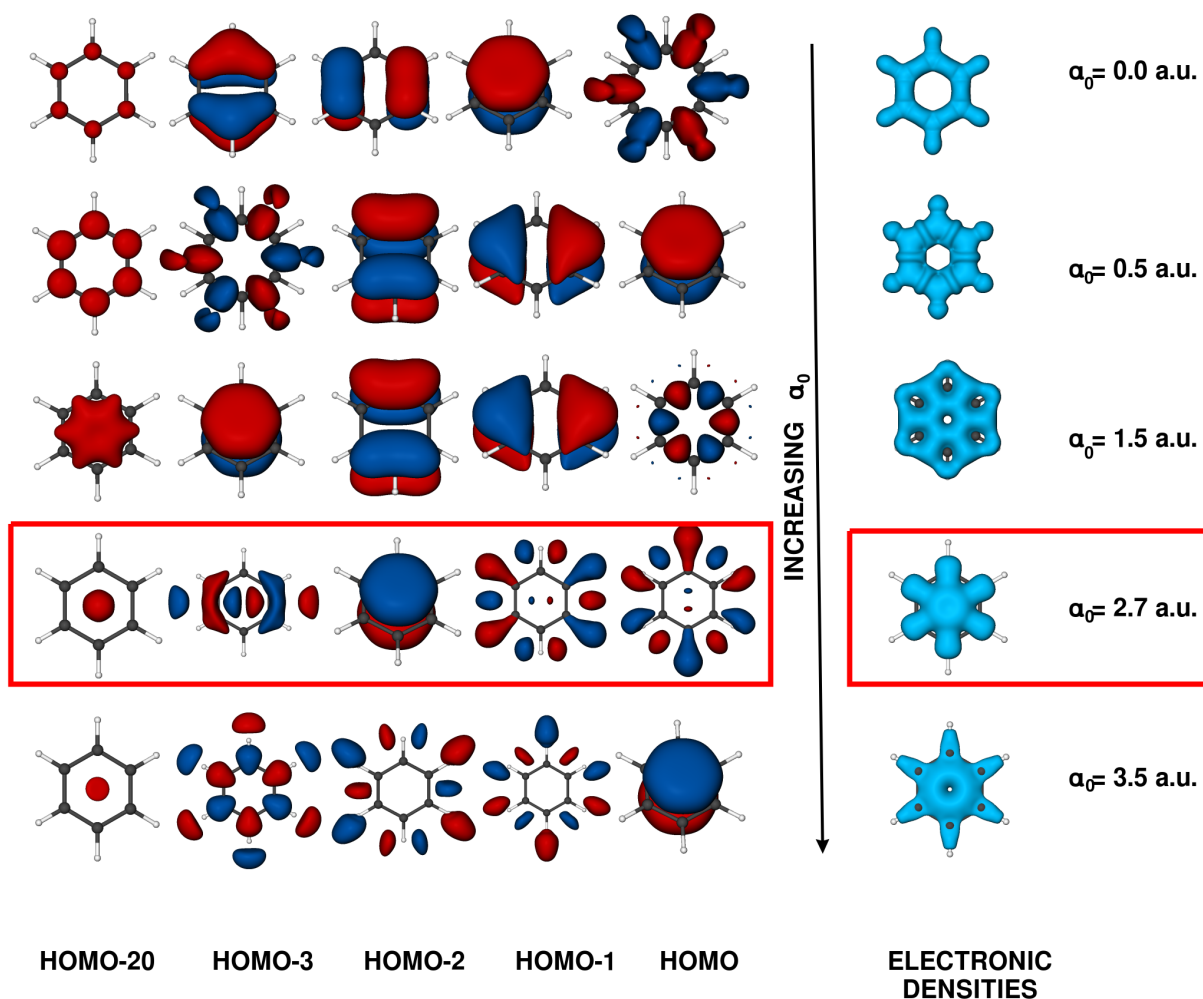


FIGURE 3.4: a) Isosurfaces of molecular orbitals and b) Electronic density of benzene (visualized using VMD) with increasing  $\alpha_0$ . The first and the last three occupied molecular orbitals (in order of increasing energy) are shown on the left side along with the total electronic density for each  $\alpha_0$  on the right side. The electronic density increases towards the center with increasing  $\alpha_0$  and is maximum at the center for  $\alpha_0 = 2.7$  a.u. (the red box). This is the same value for which we saw a deep minimum in the KH potential in the previous section. The core molecular orbital follows the exact same trend as the electronic density.

remaining occupied 15 MOs. This is exactly the same trend observed in the total HF energy plot in the previous figure. The remaining 15 MOs do not show as significant a change in energy as the core MOs. This implies that a major contribution to the change in energy of the system comes from the core orbitals of benzene. The excited state energies of the first 20 states of benzene were calculated at each  $\alpha_0$  for valence orbitals = 100 and CSFs = 2101. But their values could not be understood from the total energy curve as can be seen from Fig.(3.7). The excited state energies differed from the ground state energy by  $10^{-1} - 10^{-2}$  a.u. A plot of difference of the excited

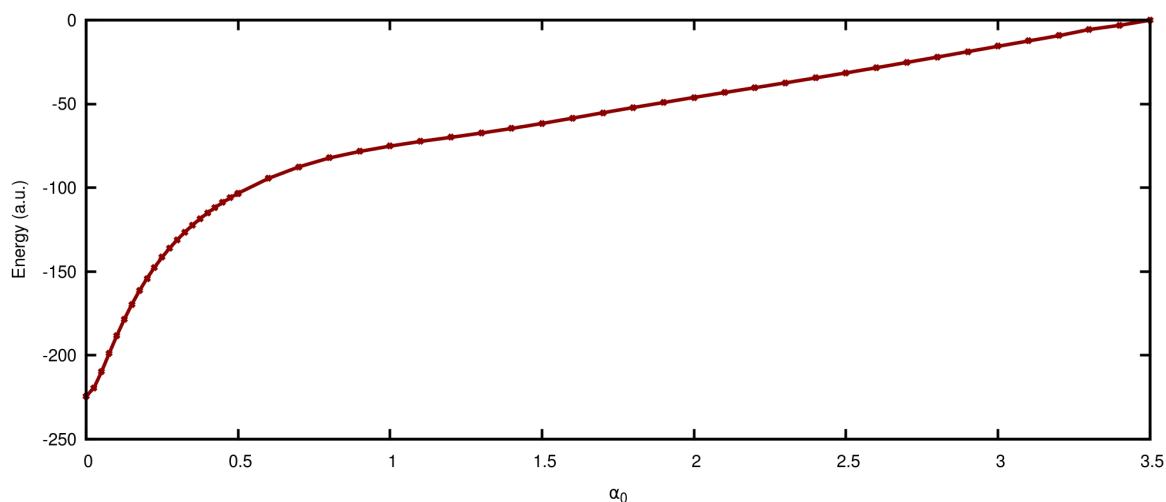


FIGURE 3.5: Hartree-Fock energies of benzene vs  $\alpha_0$  calculated using the SPD-type basis set mentioned in the previous chapter. For  $\alpha_0$  below 0.5 a.u., the energy increases rapidly as compared to the rate of increase for values greater than 0.5 a.u. As  $\alpha_0$  goes to 3.5 a.u., energy tends to 0.

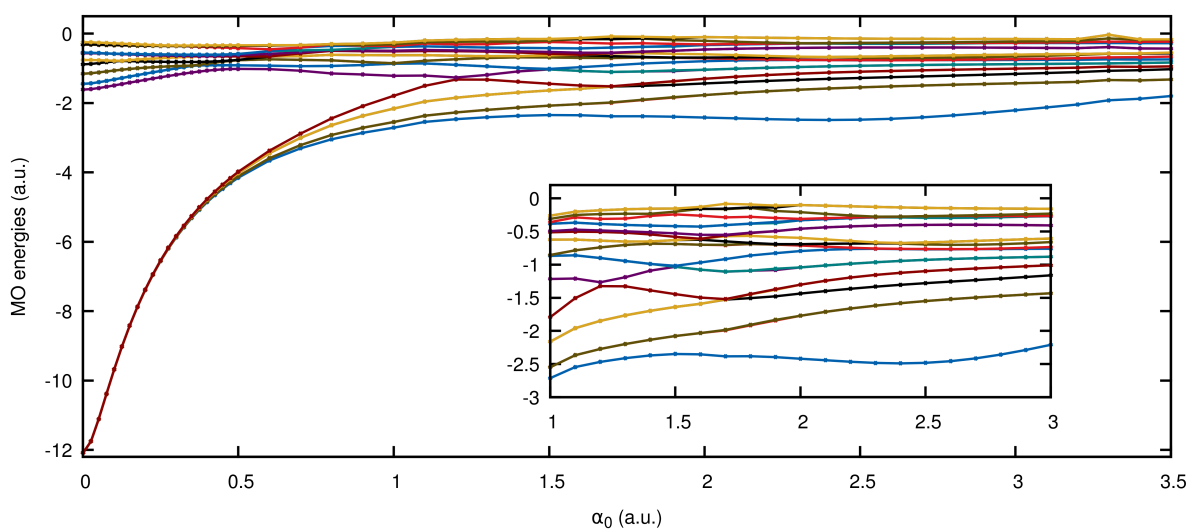


FIGURE 3.6: Orbital energies vs  $\alpha_0$ . The increase in energy in the core orbitals follows the same trend as HF energies. Relatively, the remaining occupied orbitals show a much smaller change in energy. This implies that changes in the core orbitals significantly affect the total energy of the molecule.

state energies and the ground state energies gives a better picture (Fig.(3.8)) Fig.(3.8) is a plot of the relative energies of the excited states vs  $\alpha_0$ . It shows a huge number of discontinuities which can be corrected by increasing the number of  $d$  functions and plot the energies by following the orbital overlap.

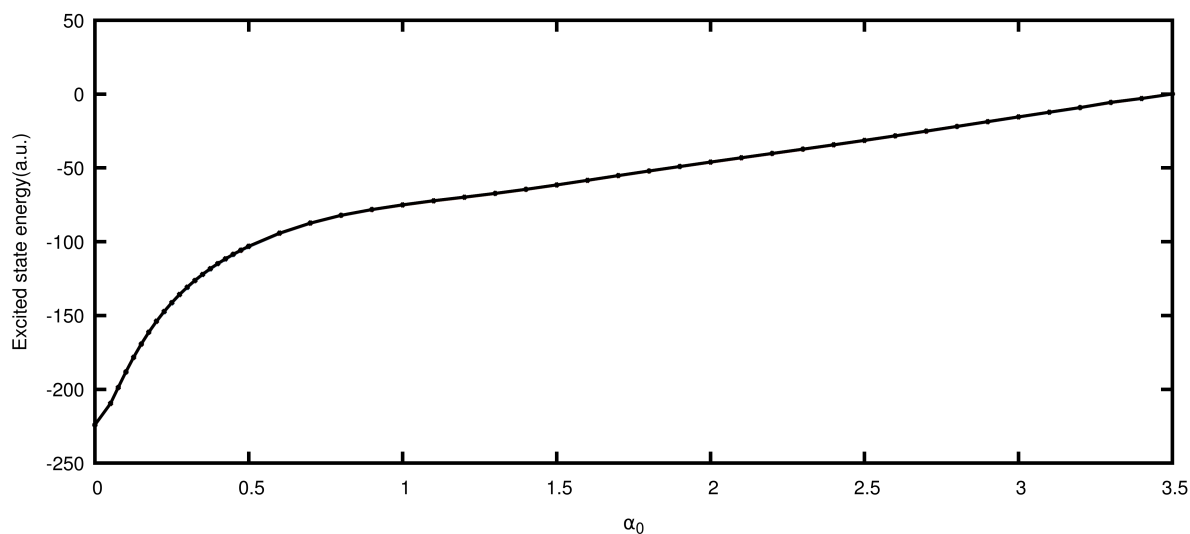


FIGURE 3.7: CIS energies as a function of  $\alpha_0$  for the first 20 singly excited states of benzene at each  $\alpha_0$ . This plot looks exactly similar to the plot of Hartree-Fock energies and does not show the excited state energies clearly. This is because the relative difference of the excited state energies is very small (of the order of magnitude -1 to -2 a.u.) compared to the magnitude of the ground state energies at each  $\alpha_0$ . Hence, it makes sense to look at the excited state energies relative to the ground state in order to understand the plot.

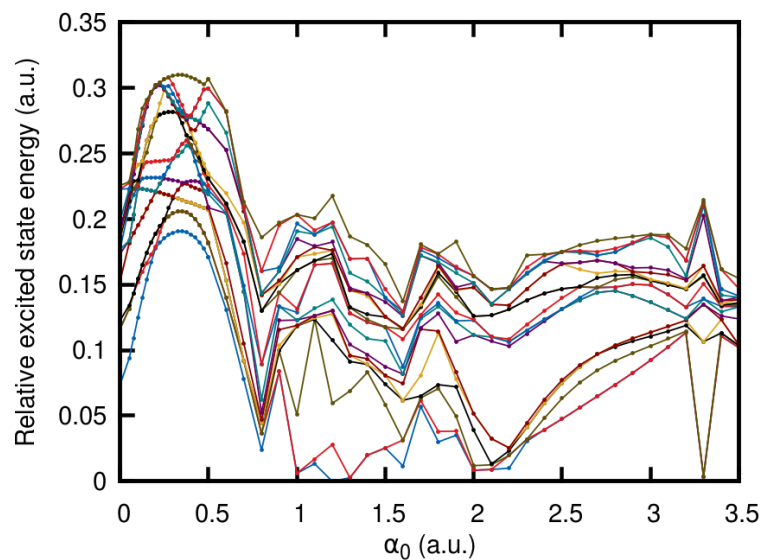


FIGURE 3.8: CIS calculations for benzene done using GAMESS and the SPD-type basis set. Number of valence orbitals were taken to be 100 and the the number of CSFs were 2101. The energies plotted here are obtained after taking a difference of the excited states with respect to the ground state. This had to be done since the range of the energies was very large compared to the increase in energies of the excited states.

## 3.2 Conclusion

The time-averaged KH potential which was observed to be a torus shaped object for a single atom was calculated for benzene at  $\alpha_0$  values close to the C-C bond distance (2.67 a.u.). A maximum was observed in the center for  $\alpha_0 = 2.7$  a.u. Electron density was also seen to be maximum near the center for this value. This suggests that the  $\pi$  electrons of benzene shift towards the center of the molecule in the presence of a circularly polarized laser.

# Appendix A

## Atomic units

Length  $a_0 = \frac{\hbar^2}{m_e e^2} = 5.29 \times 10^{-11}$  m ( $a_0$  has a unit of length)

Charge  $e = 1.602 \times 10^{-19}$  C

Energy  $E_h = 27.21$  eV = 1 Hartree

Frequency  $\nu_0 = \frac{v_0}{a_0} = 4.13 \times 10^{16}$  s<sup>-1</sup> ( $v_0$  = atomic unit of velocity)

Angular frequency  $\omega = 2\pi\nu_0 = 1.51976 \times 10^{16}$  rad/s

Electric potential  $\frac{E_h}{e} = 2.72$  V

Electric field  $E_0 = \frac{e}{4\pi\epsilon_0 a_0^2} = 5.14 \times 10^9$  V/cm

Electric field intensity =  $\frac{\epsilon_0 c E_0^2}{2} = 3.51 \times 10^{16}$  W/cm<sup>2</sup> for peak  $E_0$  field

### A.1 Energy conversion

1 eV = 8065.54 cm<sup>-1</sup>

1 kcal/mol = 0.0434 eV

# Appendix B

## SPD-type basis set

The SPD-type basis set used for helium is shown here. For the D shells, we use an even-tempered Gaussian series; the S and P shells were taken from coemd-ref although their number was modified. This same set of functions for D shells was used for carbon and hence, benzene.

### B.1 Helium

```
S 1
1 7.2133178967035583E+03 1.0000000
S 1
1 3.7392158142382218E+03 1.0000000
S 1
1 1.6182918090816222E+03 1.0000000
S 1
1 6.8024380231811381E+02 1.0000000
S 1
1 2.8186347003881883E+02 1.0000000
S 1
1 1.1708264448048692E+02 1.0000000
S 1
1 4.8127702397986326E+01 1.0000000
```

S 1  
1 1.9939284124522398E+01 1.0000000  
S 1  
1 8.1927758612694639E+00 1.0000000  
S 1  
1 3.3871337688450596E+00 1.0000000  
P 1  
1 3.2154329461467510E+00 1.0000000  
P 1  
1 1.8806445835690861E+00 1.0000000  
P 1  
1 9.5381664247686715E-01 1.0000000  
P 1  
1 4.7975023162404312E-01 1.0000000  
D 1  
1 0.0010000000 1.0000000000  
D 1  
1 0.0020000000 1.0000000000  
D 1  
1 0.0040000000 1.0000000000  
D 1  
1 0.0080000000 1.0000000000  
D 1  
1 0.0160000000 1.0000000000  
D 1  
1 0.0320000000 1.0000000000  
D 1  
1 0.0640000000 1.0000000000  
D 1  
1 0.1280000000 1.0000000000  
D 1  
1 0.2560000000 1.0000000000  
D 1  
1 0.5120000000 1.0000000000

D 1

1 1.024000000 1.000000000

D 1

1 2.048000000 1.000000000

D 1

1 4.096000000 1.000000000

D 1

1 8.192000000 1.000000000

D 1

1 16.384000000 1.000000000

D 1

1 32.768000000 1.000000000